Functionalized bacterial cellulose with tuneable porosity: a way to achieve controlled release of compounds

MSc Thesis Biotechnology

STUDENT NAME: Andra Stoica

STUDENT NUMBER: 1428985

SUPERVISOR: Panos Kopsiaftis

DATE OF SUBMISSION: 23 December 2025

Table of Contents

1. Abstract

Bacterial cellulose is an organic biocompatible compound. In the past years it has been studied for many different applications as it can serve various purposes, including the embedment and delivery of active compounds. Both these parameters are highly influenced by porosity, making the tailoring of porosity very important.

The aim of this research was to study the effect of three different carbon sources on the bacterial cellulose porosity, and to develop an inducible system that can be employed during bacterial cellulose biosynthesis to obtain different levels of porosity.

Two porosity measurements were used and compared: the mass-density method and the SEM imaging combined with ImageJ software analysis.

To achieve different levels of porosity, several genes were targeted in *Komagataeibacter sucrofermentans*: *galU*, *motA* and *motB* native genes were amplified from the target strain and assembled in a plasmid vector to achieve different levels of expression, using the inducible promoter P_{Lux}. All the different constructs were successfully obtained, but the electroporation protocol showed not to be efficient. The transformation in *K.* sucrofermentans could be performed only for a plasmid expressing the *GFPuv* gene under the P_{Lux} inducible system. This was used for a plate reader assay, with the purpose to assess the expression levels that can be achieved in this strain.

Overall, different levels of porosity, compared to wild-type bacterial cellulose, were expected: from a lower porosity, expected from overexpression of *galU*, to a higher porosity, expected from overexpression of *motA* and *motB*.

2. Introduction

Cellulose is the most abundant natural polymer on Earth, and can be produced by diverse life forms, including bacteria (Zhong et al., 2020). Bacterial cellulose (BC) is a highly pure and incredibly versatile biomaterial, produced by bacteria belonging to the *Gluconacetobacter* and *Komagataeibacter* genera. Like other cellulose counterparts, BC is an exopolymer made of β-1,4 D-glucopyranose units. The role of BC is to act as a shield, protecting bacteria from stressors such as desiccation and UV damage (Gregory et al., 2021).

BC has many properties that makes it an intriguing material for a wide variety of applications: it is completely biodegradable, non-toxic, chemically stable, biocompatible; it is characterized by high crystallinity, high hydrophilicity and water holding capacity (Betlej et al., 2021).

BC is already being studied and applied to different fields (Fig.1). In the medical field, for example, BC can be applied as a wound dressing, embedding and releasing active principles that inhibit microbial growth (de Amorim et al., 2022). In agriculture, instead, it can be used as a seed coating and embed pesticides or active compounds to protect the seed. The use of BC in this last application is novel, and the Wageningen University iGEM 2025 team, BCoated, developed for the first time a BC seed coating with tunable properties, to which this thesis project contributes. For this project, *K. sucrofermentans* DSM15973 was chosen for BC production and overexpression of native genes to alter porosity. The choice is backed by the fact that this strain was suggested to the team for its high yield and availability of protocols, mostly under the previous name of *K. xylinus* ATCC700178.

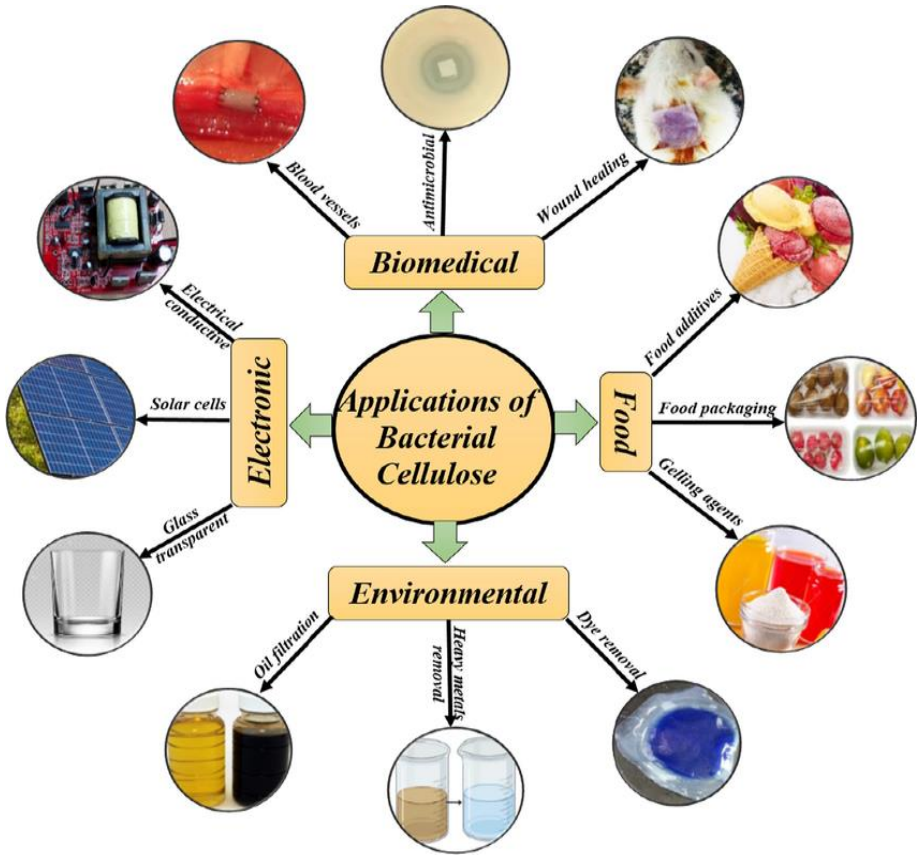

***Figure 1. General applications of bacterial cellulose in diverse fields*. Biomedical, Electronic, Food and Environmental fields are already using BC for many different purposes. However, its application is not yet present as a seed coating. Image taken from El-Gendi et al., 2022.**

The high water holding capacity of BC could help the embedment of substances and it is directly proportional to the surface area and pore volume in the matrix (Swingler et al., 2021), making porosity an important parameter and subject of this study.

The release rate of compounds can indeed be tailored by controlling the porosity of bacterial cellulose (Ullah et al., 2016) and improving the porosity of bacterial cellulose is critical for immobilizing and storage of various compounds (Ashrafi et al., 2019).

Some native genes have already shown, when overexpressed in certain *Komagataeibacter* strains, the ability to alter porosity. One of these genes is *galU* (Fig. 2): it is an essential gene that controls the carbon metabolic flux between the bacterial cellulose synthesis pathway and the pentose phosphate (PP) pathway (Huang et al., 2020). The BC production pathway (Fig.2) starts with glucose-6-phosphate, which is isomerized to glucose-1-phosphate by phosphoglucomutase (EC 5.4.2.2). Then, glucose-1-phosphate reacts with UTP, forming uridine-5′-diphosphate-α-D-glucose (UDP-glucose) in a reaction catalyzed by *galU* through its UTP-glucose-1-phosphate uridylyltransferase activity (EC 2.7.7.9). Finally, the cellulose synthase complex (BCS, EC 2.4.1.12) transfers glucosyl residues from UDP-glucose to the nascent BC chain (Fig. 2) (Römling & Galperin, 2015).

In a previous study in *K. xylinus*, *galU* was overexpressed and targeted through CRISPRi: as a result, the porosity of bacterial cellulose was found to be negative with the expression level of *galU* (Huang et al., 2020).

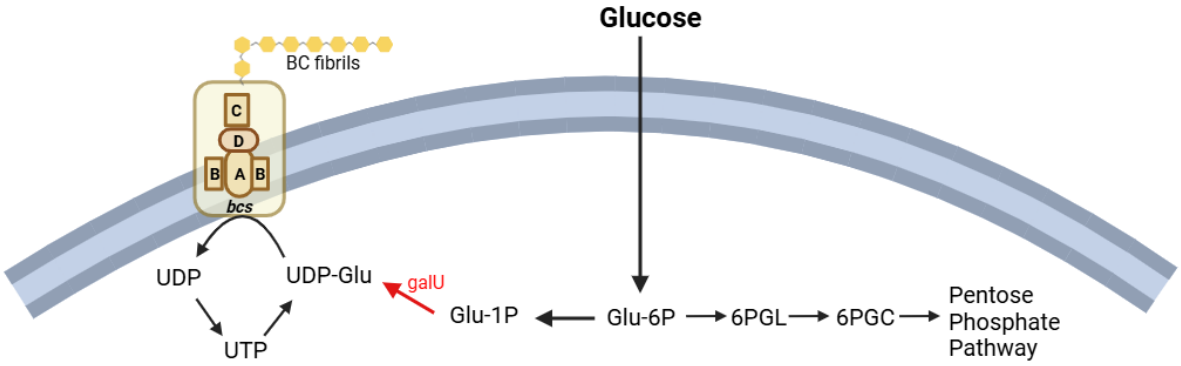

***Figure 2. BC production pathway. galU*, here highlighted, directly participates in the BC production pathway, by taking part in the conversion of Glucose-1-P into UDP-glucose. Then, the cellulose synthase (*bcs*) transfers the glucosyl residues from the UDP-Glucose to the nascent β-D-1,4-glucan chain (Römling & Galperin, 2015). Image created using BioRender.**

Two other interesting native genes, both targeted in these experiments, are *motA* and *motB*, associated with motility. Bacterial motility is a phenomenon involved in biofilm formation (Bogino et al, 2013). This is seemingly the result of chemotaxis, which is the movement by which bacteria react to the changing chemical composition of their surroundings, to approach chemically beneficial environments and avoid non-beneficial environments (Tamar et al., 2016). The *Komagataeibacter* genus exhibits chemotactic movement (Basu et al., 2018) (Jacek et al., 2019).

The cell motility rate in *K. hansenii* correlates with biosynthesis and extrusion of BC microfibrils (Brown et al., 1976). In another study, it was reported that the *motA* and *motB* overexpression in *K. hansenii* ATCC 23769 resulted in bacterial cellulose with enlarged pores compared to wild type was obtained (Jacek et al., 2019). A BLAST analysis confirmed that *motA* and *motB* genes are also present in *K. sucrofermentans* DSM15973.

The expected outcome of overexpressing these three target genes is summarized in Figure 3.

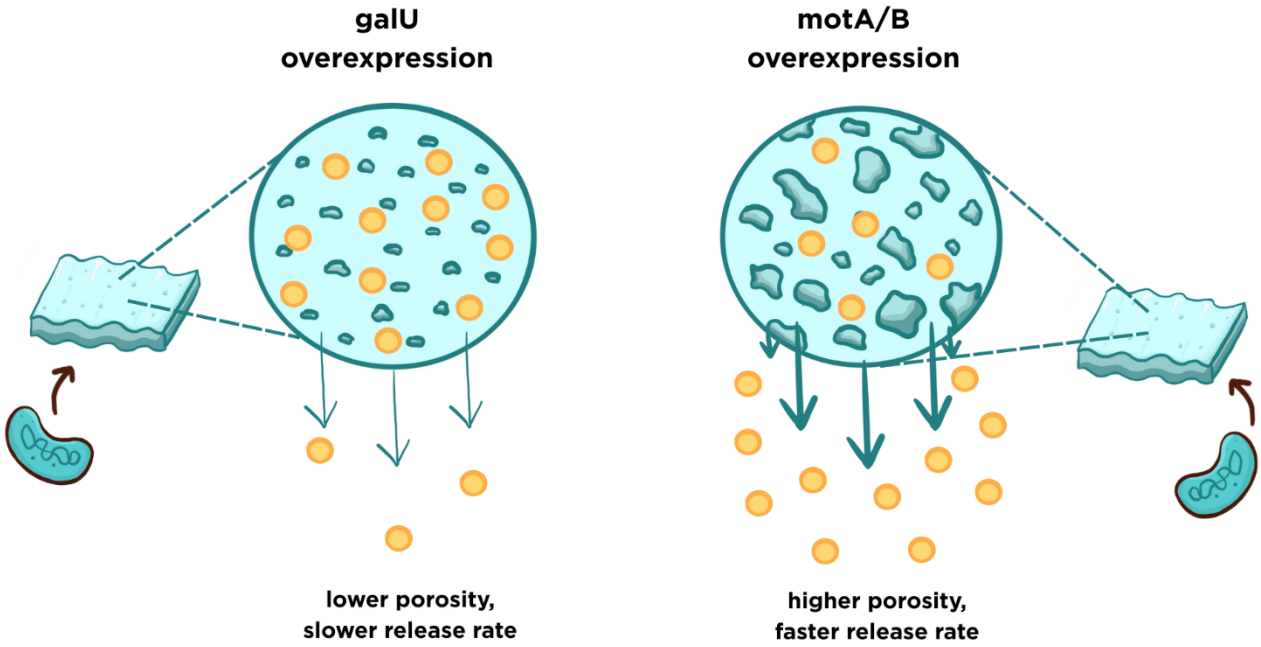

Figure 3. Expected outcomes of overexpressing galU and motA/B. **By overexpressing *galU*, *K. sucrofermentans* is expected to produce a BC with lower porosity and, as a result, the embedded compounds would be released at a slower rate. By overexpressing *motA*, *motB* or both genes at the same time, *K. sucrofermentans* is expected to produce a BC with increased porosity and result in a higher release rate of embedded compounds.**

To achieve different levels of overexpression, these three native genes were expressed under the P_{Lux} inducible system in the pSEVA331 backbone. Both the backbone and the promoter, induced by HSL, showed in a previous study to perform well in *K. sucrofermentans* DSM15973 (previously named *Gluconacetobacter xylinus* ATCC 700178), ensuring strong expression and low leakiness (Teh et al., 2019).

In a previous study in *G. hansenii*, BC grown on different carbon sources showed different porosity. The fructose-grown samples showed the highest porosity, while glucose-grown samples showed the lowest porosity (Ashrafi et al., 2019). For these experiments, wild type BC was grown on different carbon sources, namely glucose, fructose and sucrose. This was done to test another approach to change porosity and compare the results with the native genes' overexpression.

To measure porosity, two methods were used and compared: the mass density method and the SEM imaging analysis through ImageJ software. The mass density method is a simple and versatile way to assess porosity, in which the mass and density of ice are used for the porosity calculation of the freeze-dried samples (Hossen et al., 2020). SEM was chosen as an additional method for the fact that image analysis allows the quantification of the morphological aspect and the measurement of the size of the pores (Andreola et al., 2000).

Overall, the aim of these experiments is to achieve tunable BC porosity in *K. sucrofermentans* DSM15973, investigating if the HSL-induced expression of *galU* can

decrease porosity, and whether the expression of *motA* and *motB* can lead to larger porosity. Last, the effect of multiple carbon sources was investigated for its impact on porosity.

3. Materials and Methods

3.1 Bacterial strains and Media.

K. sucrofermentans was purchased from DSMZ (Product number: DSM 15973) and was used for BC production and for transformation. *E. coli* Stbl4 cells (ElectroMAX™ Stbl4™ Competent Cells, Invitrogen™) were used for general molecular cloning. *K. sucrofermentans* cells were grown on YPD (Yeast Extract Peptone Dextrose) medium, containing 25 g/L glucose, 10 g/L bacteriological peptone and 10 g/L yeast extract. pH was adjusted to 6.5 using citric acid. The pH of the media was measured either with pH-meter or with pH indicator strips (MQuant, pH indicator strips, pH 0-14, Universal Indicator) when measuring after bacterial inoculation. To test the effect of different carbon sources, the YPD medium preparation protocol was modified, and glucose was substituted with fructose or sucrose in the same concentration. From the glycerol stock, *K. sucrofermentans* was inoculated in 10 mL YPD medium with 0.2% cellulases (Cellulases from *T. reesei* ATCC26921, Sigma-Aldrich) and grown for at least 48 hours at 30 °C, before either being used for BC production or transformation. *E. coli* Stbl4 cells were routinely grown overnight at 30°C in LB (Luria Broth) medium, provided with antibiotic. After cloning, the cells were plated on LB agar plates with antibiotic (25 µg/mL chloramphenicol).

Where appropriate, chloramphenicol was added: 185 µg/mL for *K. sucrofermentans*, 25 µg/mL for *E.Coli*.

M9 minimal medium was used for the plate reader assay, containing 58 g/L Na2HPO4, 30 g/L KH2PO4, 5 g/L NaCl, 246.47 g/L of MgSO4, 73.5 g/L of CaCl2, 132.14 g/L of (NH4)2SO4 and 25 g/L glucose.

3.2 Gibson Assembly.

The inducible P_{Lux} gene expression was carried out by constructing 5 plasmids based on the pSEVA331 backbone and assembled using Gibson assembly method. The *in silico* cloning was performed using SnapGene, creating the following constructs: pSEVA331-P_{Lux}-*GFPuv*, pSEVA331-P_{Lux}-*galU*, pSEVA331-P_{Lux}-*motA*, pSEVA331-P_{Lux}-*motB*, pSEVA331-P_{Lux}-*motA*-*motB* (Fig.4)

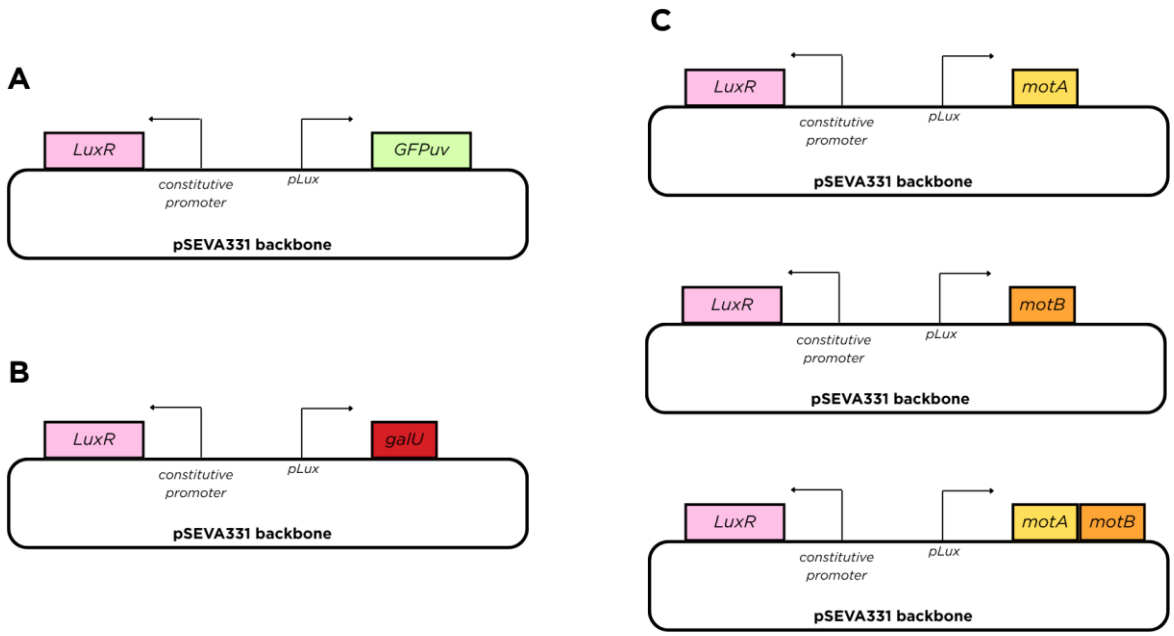

***Figure 4. Maps of the assembled plasmids*. The plasmids contain the *LuxR* gene under the J23104 constitutive promoter, and the target genes under the P_{Lux} inducible promoter and the B0034 RBS (BBa_B0034). (A) pSEVA331- P_{Lux}-*GFPuv*, used to assess P_{Lux} efficiency and HSL working concentrations in *K. sucrofermentans*. (B) pSEVA331-P_{Lux}-*galU*, expected to decrease porosity upon induction of *galU* overexpression. (C) pSEVA331-P_{Lux}-*motA*, pSEVA331-P_{Lux}-*motB* and pSEVA331-P_{Lux}-*motA-motB*, expected to increase porosity upon induction of *motA* or *motB* or both. In the pSEVA331-PLux-*motA-motB* plasmid, the native RBS was used for *motB*.**

To amplify *galU*, *motA*, *motB* and *motA-motB*, *K. sucrofermentans* genome was first isolated using the DNeasy Blood and Tissue kit (QIAGEN), following the handbook instructions for Gram negative bacteria, extending the 65°C step for 3 hours and including the optional RNAse A step. The final elution step was performed using 100 µL of elution buffer.

The amplification of *galU*, *motA*, *motB* and *motA-motB* from *K. sucrofermentans*, and the amplification of the desired fragments from pSEVA331 and pSEVA64-*gfpuv*-wt, were performed using the (Q5® High-Fidelity DNA Polymerase, New England Biolabs). A 927 bp fragment was ordered from Genscript to complete the assembly, as the pSEVA64-*gfpuv*-wt plasmid missed that fragment. The amplified fragments were run on 1% agarose gel at 100V for 35 min.

The fragments were isolated from the agarose gel using the Zymoclean Gel DNA Recovery Kit (ZYMO research), following the protocol provided in the kit.

All amplified fragments were assembled using Gibson assembly (NEBuilder® HiFi DNA Assembly Master Mix, New England Biolabs. Assembly reaction: 50°C for 15 min) and introduced through electroporation in electrocompetent *E. coli* Stbl4 cells. 20 µL of electrocompetent cells were mixed with 1 µL plasmid and pulsed via an electroporate set at

2.5 kV, 200 Ω, 25 µF. 1 mL of SOC Outgrowth Medium (NEB #B9020S) was then immediately added. The resuspended cells were transferred to a 15 mL sterile falcon tube and incubated at 30ºC for 1 hour and 30 minutes, while shaking. Afterwards, the cells were transferred in a sterile 1.5 mL Eppendorf tube and spin down for 3 minutes at 2000 rcf. 800 µL of supernatant were removed and the pellet with remaining medium was resuspended and plated on LB agar plates with antibiotic.

To allow electroporation, *K. sucrofermentans* was first made electrocompetent. 1 mL of OD_{600}=0.8 culture was transferred to a sterile Eppendorf tube and centrifuged for 2 minutes at 5500 rpm. The supernatant was removed and the pellet was resuspended with 1 mL of pre-cooled 10% glycerol. These steps were performed a second time, with the final pellet resuspension in 100 µL of pre-cooled 10% glycerol. 500-1200 ng plasmid were added to this final resuspension and incubated for 5-10 minutes on ice. Then, the cells were pulsed via an electroporate set at 2.5 kV, 400 Ω, 25 µF. After adding 1 mL YPD recovery medium (2.5% glucose, 2% cellulases), the cells were transferred to 15 mL sterile falcon tubes and incubated at 30°C for at least 4 hours, while shaking. Afterwards, the cells were transferred in a sterile 1.5 mL Eppendorf tube and spin for 5 minutes at 5500 rpm. 800 µL of supernatant were removed and the pellet with remaining medium was resuspended and plated on YPD agar plates with antibiotic.

To ensure the inserts were present, colony PCR was performed using (OneTaq Hot Start 2X Master Mix with Standard Buffer, NEB #M0484) following the protocol provided by the product company (25 µL reaction) and confirmed with gel electrophoresis. A set of internal primers, targeting the strain-specific *bcsA* gene, was used to confirm the successful electroporation of *K. sucrofermentans*.

All the obtained plasmid constructs were additionally confirmed by Macrogen Sanger sequencing and Plasmidsaurus plasmid sequencing.

All the templates' features are displayed on Table S1, while the primers and their sequences are provided on Table S2 (Supplementary).

3.3 P_{Lux} induction.

To test the P_{Lux} activity and the range of concentrations at which HSL induction happens, a fluorescence 96-well plate reader assay was performed on *K. sucrofermentans* transformed with the pSEVA331-P_{Lux}-GFPuv plasmid. Liquid cultures were first incubated overnight with cellulases and chloramphenicol. A transparent 96-well plate was used, containing the samples in triplicates and, in the first column, M9 minimal medium as a negative control.

A target OD_{600} of 0.1 was used for each well, containing resuspended *K. sucrofermentans* cells in M9 minimal medium with HSL (N-Hexanoyl-L-homoserine lactone, CAS 147852-83-3) in different concentrations between 0.1 and 200 µM. Additionally, 50 µL of mineral oil were added on top of each well. The complete plate layout is provided in Figure 5.

The microplate reader Neo 2 (Agilent BioTek Synergy Neo2 Hybrid Multi-Mode Microplate Reader) was used to measure the OD_{600} and fluorescence (395 nm excitation max, 509 nm emission max). The obtained values were evaluated, and two duplicates were taken for the

data analysis, in which all the values were subtracted from the negative control (M9 medium not inoculated with cells).

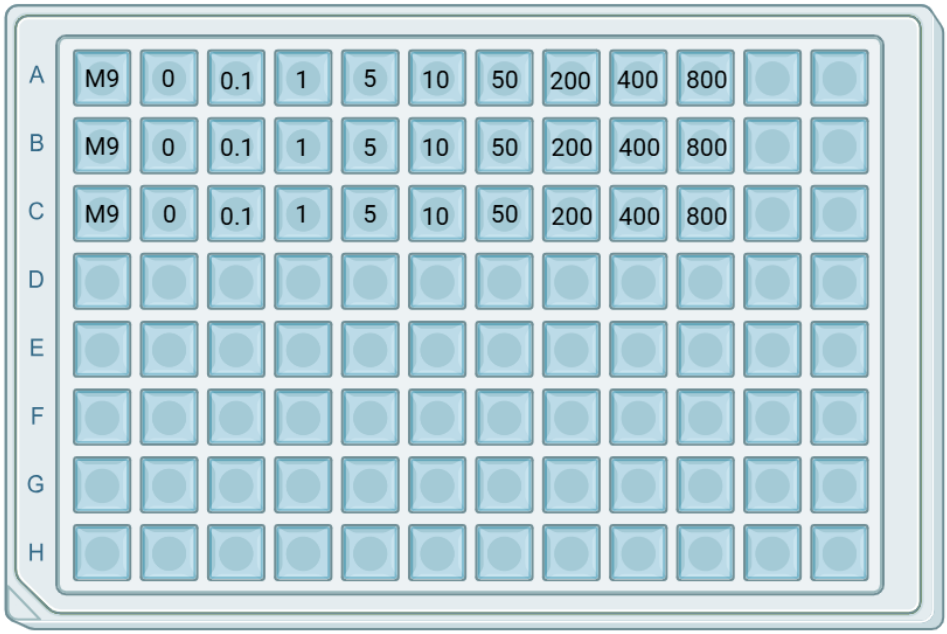

***Figure 5. 96-well plate layout*. The samples are measured in triplicated, with concentrations expressed in µM. Created using BioRender.**

3.4 BC production.

To produce BC, a 10% v/v of OD_{600} 0.3 *K. sucrofermentans* culture was added in each Erlenmeyer flask, containing YPD medium (pH 6-6.5) or the equivalent with different carbon source (fructose or sucrose). The flasks were incubated for 72 hours at 30°C statically. Afterwards, BC sheets were collected, rinsed and washed in 0.1 M NaOH for one hour at 80ºC.

Lint-free tissues were used to remove the surface water from the washed BC, before freezing it at -20°C overnight and continuing with the protocol for porosity measurement.

3.5 Porosity measurement.

Porosity was first measured using the mass-density method, following a protocol based on previous literature (Hossen et al., 2020). The frozen weight was recorded with an analytical balance, before freeze-drying overnight. After collecting the BC from the freeze-dryer, its dry weight was recorded, and the porosity could be assessed. The obtained data was used to determine the bulk density and, from the obtained value, the porosity.

Bulk density: $\rho_b = \frac{w_c}{\frac{w_c}{\rho_c}+\frac{w_i}{\rho_i}}$

Where Wc is the freeze-dried weight of cellulose nanofibrils (CNF) ρc is density of CNF (assumed to be 1.5 g/cm3), Wi = mass of ice in the sample calculated from the mass difference of the frozen and the freeze-dried (degassed) samples, and ρi = density of ice (0.92 g/ cm3).

Porosity: $P = 1 - \frac{\rho_b}{\rho_c}$

Additionally, for some of the wild-type BC samples grown on different carbon sources, the average pore area was measured using Scanning Electron Microscopy (SEM). The BC samples were prepared and imaged by the Wageningen Electron Microscopy Center. Before the analysis, our BC was cut into smaller pieces. Samples of approximately 1 cm^2 were attached to aluminium stubs with double-sided carbon tape and were sputter coated with approx. 10 nm tungsten from above and tilted at +45 degrees and -45 degrees (SCD 500, Leica, Vienna, Austria). The imaging was performed using a Field emission scanning electron microscope (Magellan 400, Thermo-Fischer/FEI, Eindhoven, the Netherlands). SEM specs: 2.00kV, 13pA.

ImageJ software was used to analyze SEM images, determining the pores' size. A scale was first set by measuring the length of the provided µm scale in pixels. Afterwards, the images were cropped. Binarization is a required step, in which the image is divided into foreground and background (ImageJ, 2020), allowing to isolate the object of interest (in this case, the pores). The binarization of the images was performed by adjusting the threshold to cover all the pores in red, while leaving the BC fibrils in gray. The Analyze Particles tool allowed the determination of the areas of the different pores in the pictures.

4. Results

4.1 BC production on different carbon sources.

After 3 days of inoculation, 5 BC sheets for each condition were produced. Qualitatively, the glucose-grown BC sheets looked more uniform, while the fructose-grown sheets were thicker. The sucrose-grown sheets showed to be the thinnest, most transparent and least uniform among the three conditions.

The pH of the three different cultures shifted from 6.5 to the following: pH 3 glucose, pH 5 fructose, pH 3.5 sucrose. The OD_{600}, instead, increased as follows: 0.43 OD_{600} glucose, 0.58 OD_{600} fructose, 0.09 OD_{600} sucrose. Overall, the fructose sample showed the thickest cellulose, the lowest change in pH in the medium and the highest OD_{600} after three days.

Through the mass-density method, the porosity of the glucose samples shifted from 98.6% to 99.1%. The measured average was 98.2% porosity.

For the fructose samples, the porosity shifted from 98.1% to 99%, with an average of 98.6% porosity.

For the sucrose samples, the porosity shifted from 97.5% to 98.3%, with an average of 98% porosity.

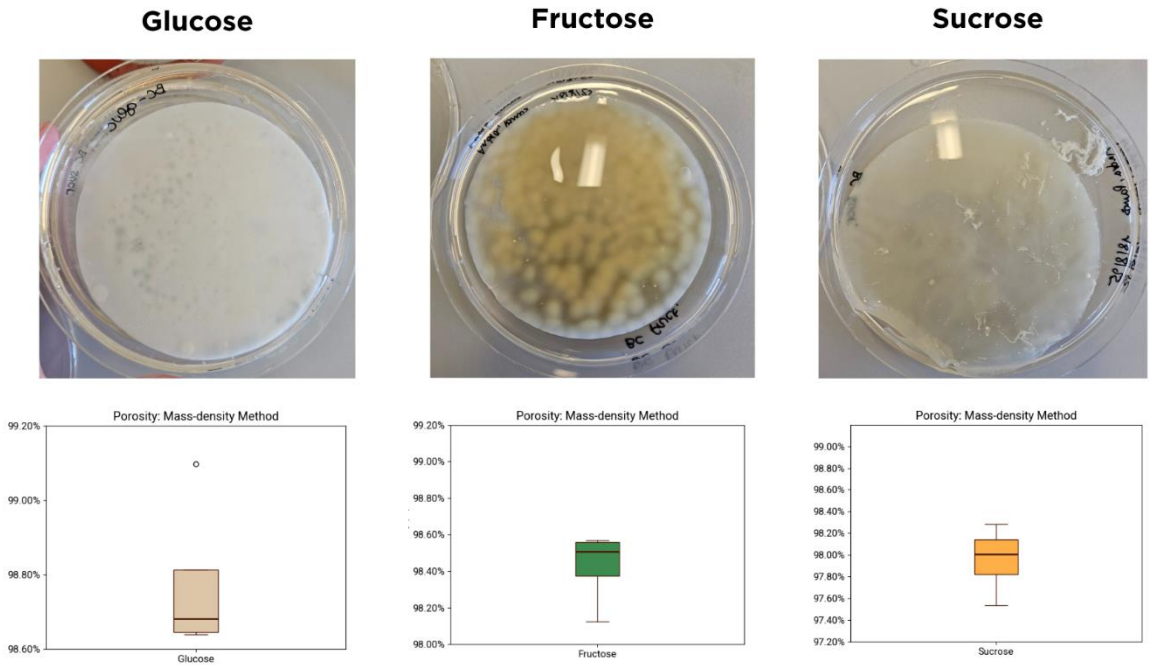

***Figure 5. BC grown on different carbon sources and porosity boxplots*. On top, the images show that BC looks qualitatively different when grown on different carbon sources. On the bottom, the boxplots represent the distributions of porosity.**

Through SEM analysis, 6 images were taken for 4 samples: two glucose-grown samples of different porosities (98.4% and 96.1% respectively), one sample grown on fructose (99% porosity) and one sample grown on sucrose (98.2% porosity).

For the two glucose samples, the higher porosity of the first sample was reflected in a higher average pore area, indicating a correlation between the two types of measurements. Notably, these samples derive from cultures cultivated at a lower pH (starting pH 5.5), therefore the comparison may be inaccurate.

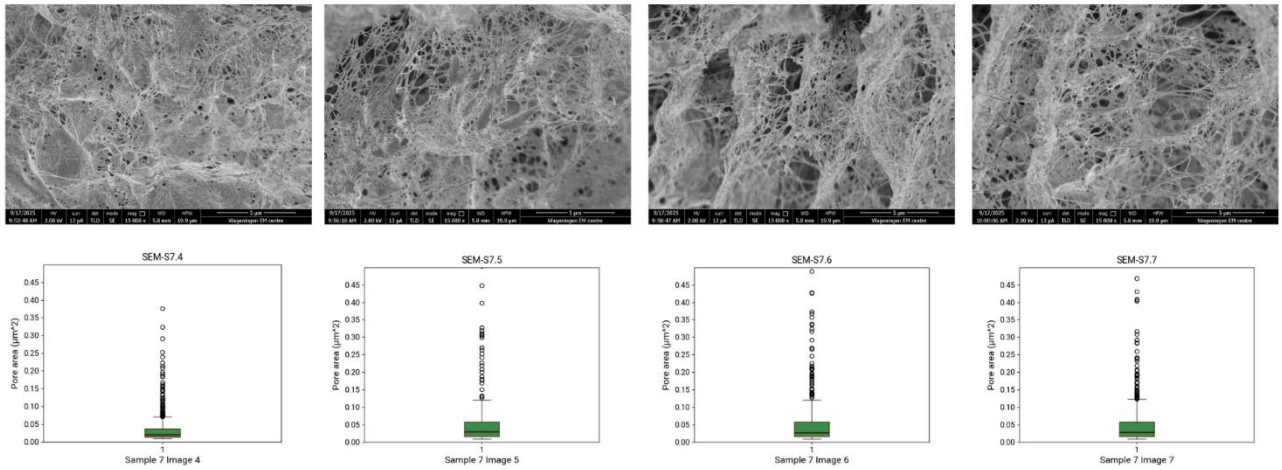

***Figure 6. SEM images and boxplots Glucose-grown sample 1*. The measured areas of the pores are summarized in a boxplot at the bottom of the respective picture. Four images of the same sample were analyzed though ImageJ and used to determine the average pore area of the sample (0.063µm^2), after determining the average pore areas of the singular images: 0.036, 0.052, 0.100 and 0.0065 µm^2. A t-test, however, determined the significance of the measurements, rejecting the null hypothesis for which there is no difference among the images (p=4.69x10^{-6}).**

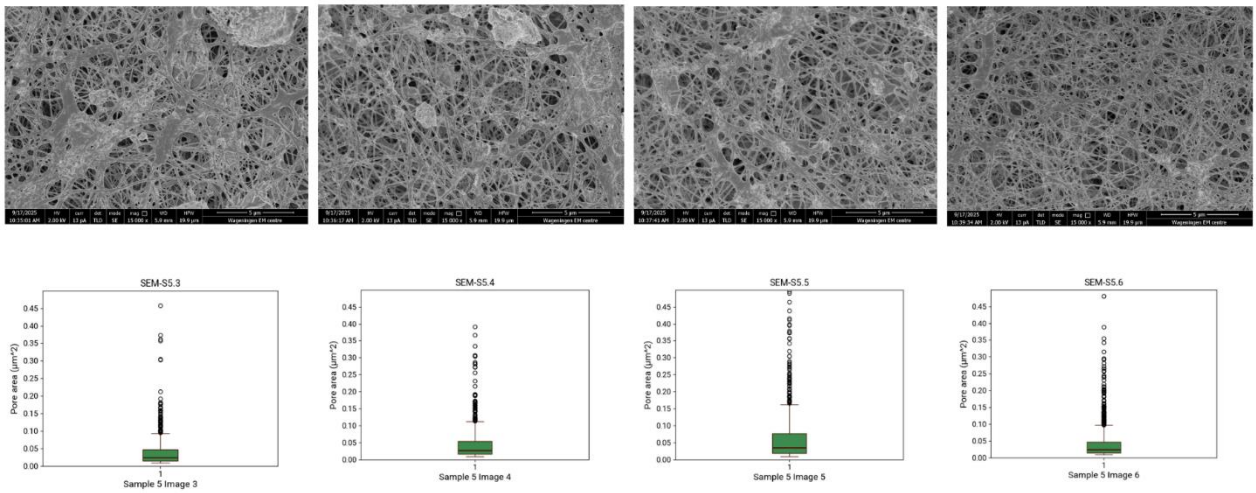

***Figure 7. SEM images and boxplots Glucose-grown sample 2*. The measured areas of the pores are summarized in a boxplot at the bottom of the respective picture. Four images of the same sample were analyzed though ImageJ and used to determine the average pore area of the sample (0.048 µm^2), after determining the average pore areas of the singular images: 0.065, 0.044, 0.045 and 0.0040 µm^2. A t-test, however, determined the significance of the measurements, rejecting the null hypothesis for which there is no difference among the images (p= 6.97x10^{-19}).**

The average pore area of the fructose-grown sample (Fig.8) was lower than the average pore area of both glucose-grown samples.

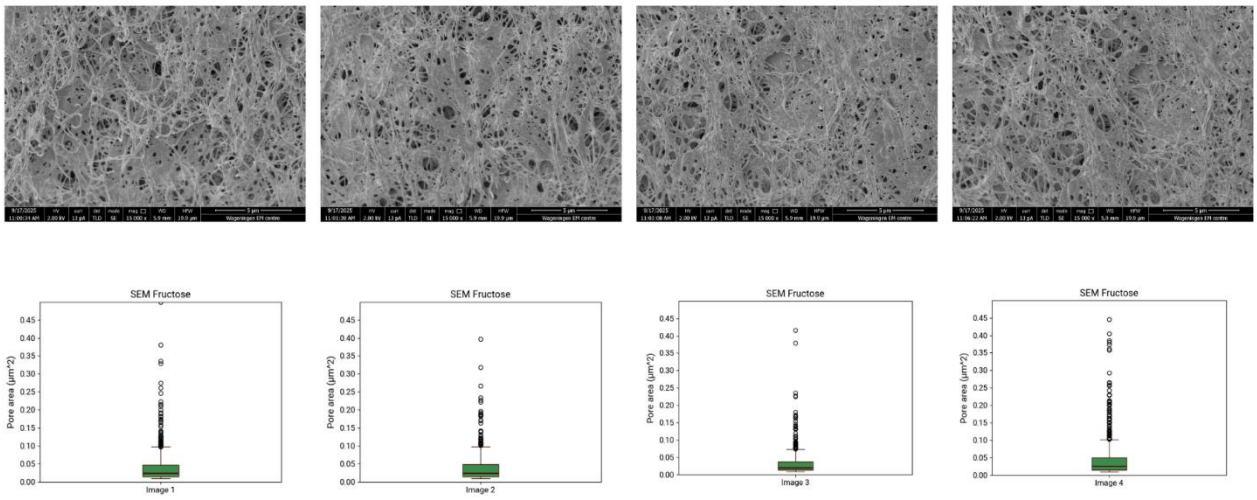

***Figure 8. SEM images and boxplots of the Fructose-grown sample*. The measured areas of the pores are summarized in a boxplot at the bottom of the respective picture. Four images of the same sample were analyzed though ImageJ and used to determine the average pore area of the sample (0.041 µm^2), after determining the average pore areas of the singular images: 0.041, 0.041, 0.034 and 0.046 µm^2. A t-test, however, determined the significance of the measurements, rejecting the null hypothesis for which there is no difference among the images (p= 3.39x10^{-4}).**

The sucrose-grown sample would have been expected to have a similar average pore area as the first glucose sample (0.063 µm^2). Nevertheless, the measured average pore area though ImageJ was 0.043 µm^2, slightly higher than the fructose-grown sample.

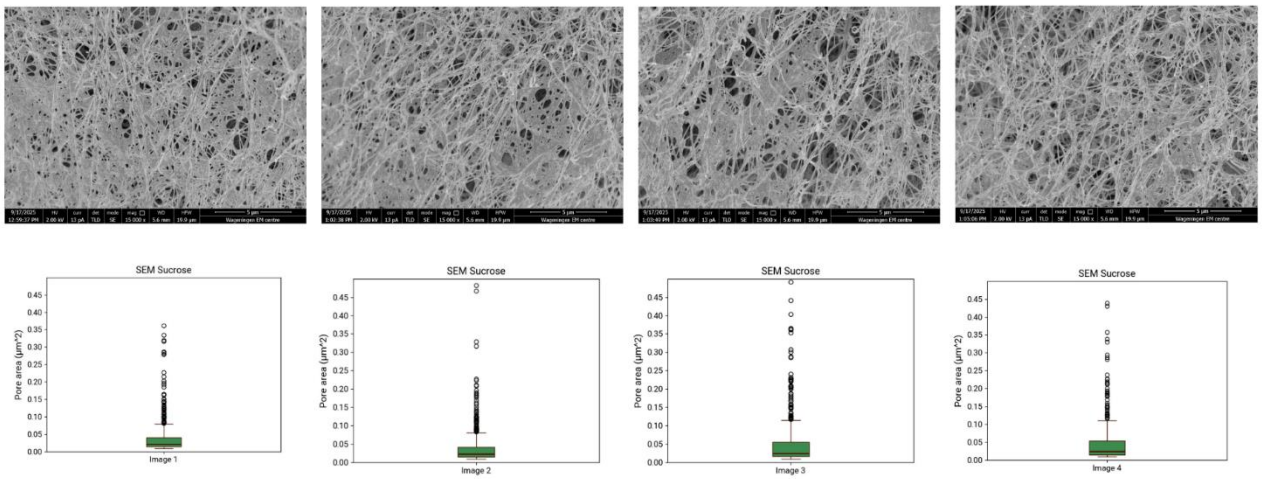

***Figure 9. SEM images and boxplots of the Sucrose-grown sample*. The measured areas of the pores are summarized in a boxplot at the bottom of the respective picture. Four images of the same sample were analyzed though ImageJ and used to determine the average pore area of the sample (0.043 µm^2), after determining the average pore areas of the singular images: 0.052, 0.037, 0.038 and 0.043 µm^2. A t-test, however, determined the significance of the measurements, rejecting the null hypothesis for which there is no difference among the images (p= 4.74x10^{-6}).**

4.2 Plasmid construction.

The desired fragments were successfully amplified and isolated from the agarose gel. Subsequently, Gibson assembly was performed.

Colony PCR and sequencing showed, in the electroporated *E. coli*, the successful Gibson assembly of pSEVA331-P$_{Lux}$-*GFPuv* plasmid (Fig. 9).

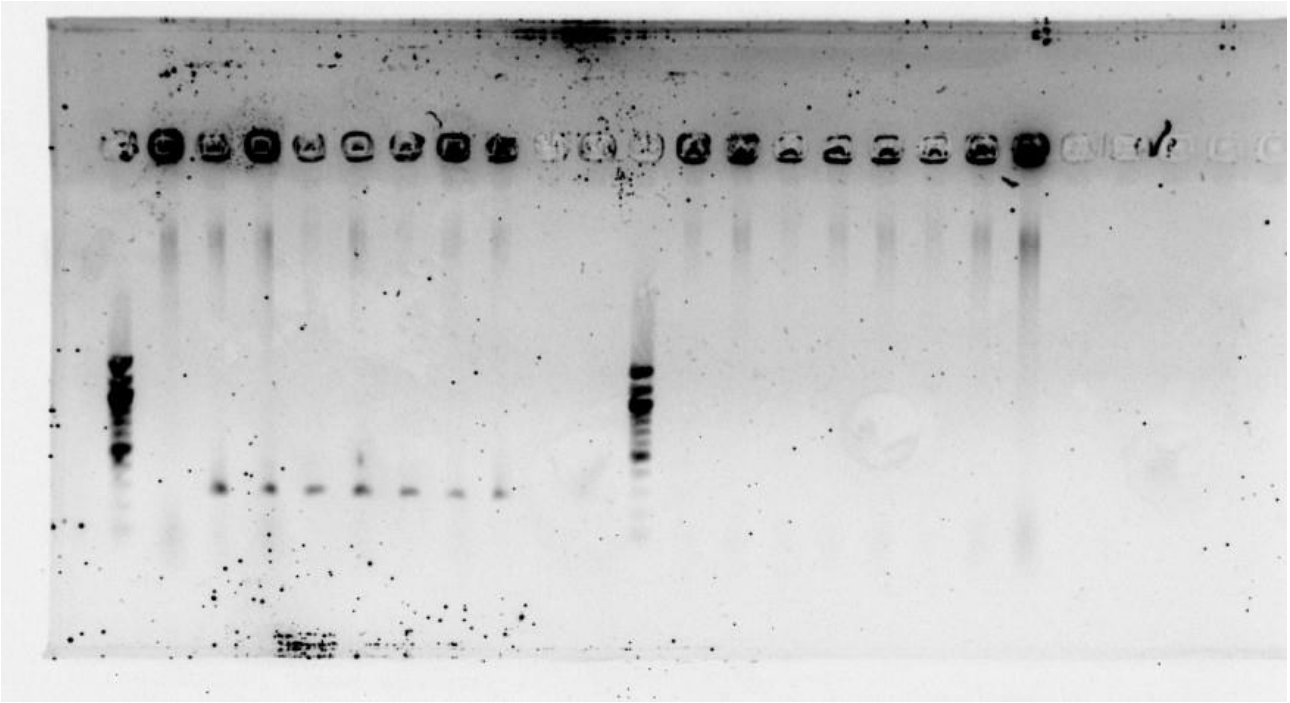

***Figure 10. colony PCR (OneTaq) of pSEVA331-P_{Lux}-GFPuv*. The ladder (GeneRuler 100 bp DNA ladder) indicates that 7 samples showed the desired 246 bp amplified band. Primers used: Gibson_fw + Gibson_rv**

Colony PCR of both plasmid (Figure 10) and *bcsA* gene (Figure 11), showed successful electroporation of pSEVA331-P_{Lux}-*GFPuv* in *K. sucrofermentans*.

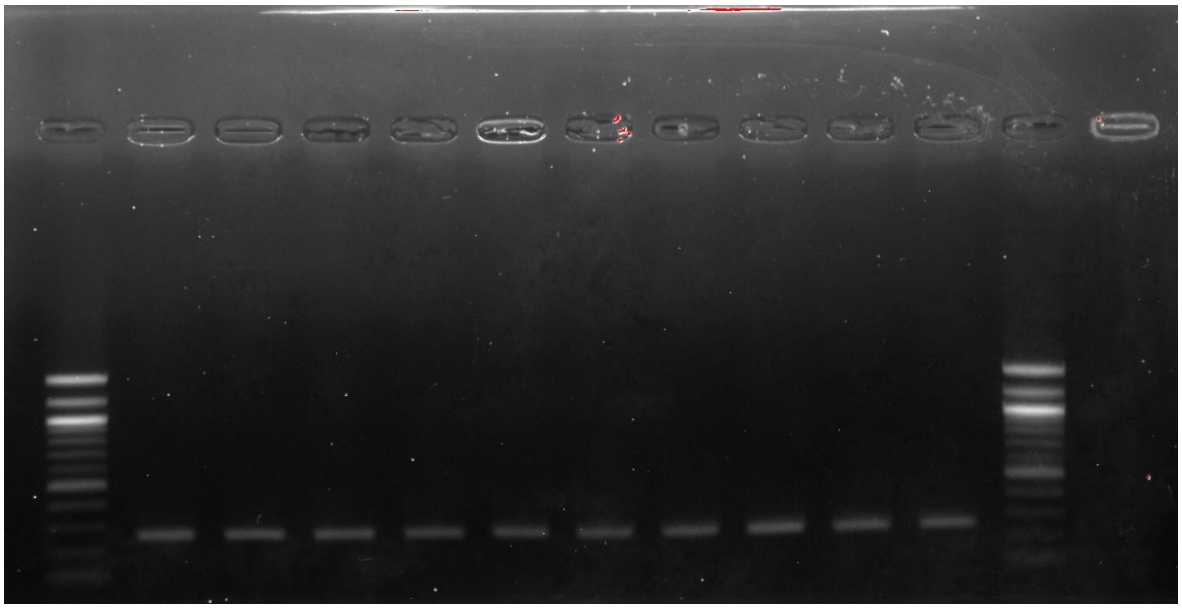

***Figure 11. Colony PCR of transformed K. sucrofermentans with pSEVA331-P_{Lux}-GFPuv.* By using the primers Gibson_gal/mot_fw and Gibson_P_{Lux} _rv, a 246bp fragment could be amplified for each sample, confirming the presence of the desired plasmid.**

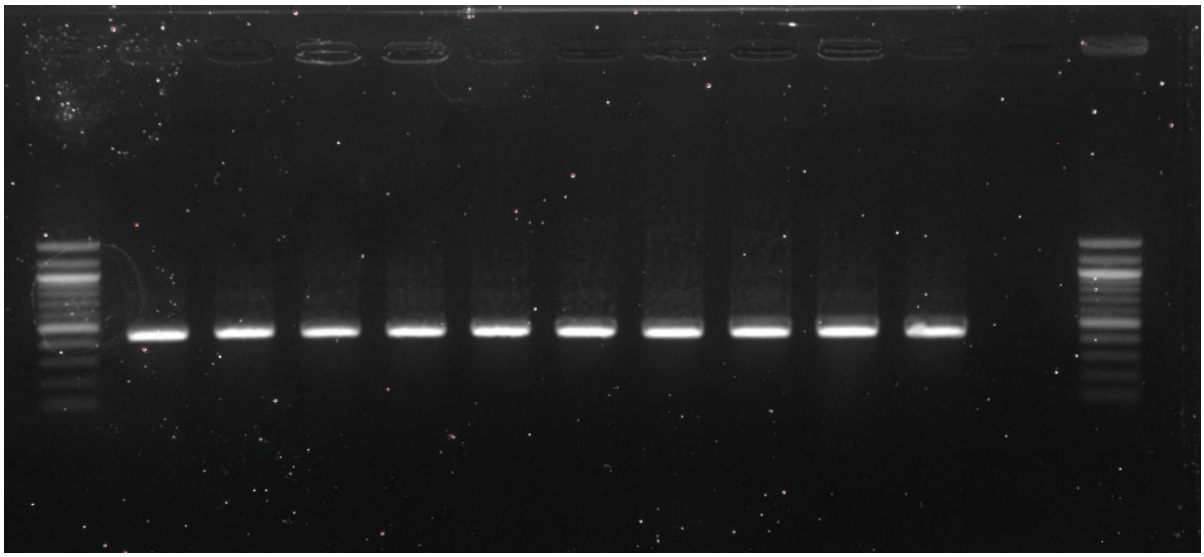

Figure 12. Colony PCR of bcsA in the transformed K. sucrofermentans with pSEVA331-P_{Lux}-GFPuv. **By using strain-specific bcsA_fw and bcsA_rv primers, a 400bp fragment (GeneRuler 100bp DNA ladder) could be amplified for each sample, confirming the successful electroporation of the strain.**

After genome isolation, *galU*, *motA*, *motB* and *motA-motB* were amplified, and isolated from the agarose gel. Then, they were assembled in pSEVA331-P_{Lux}-*GFPuv*.

All the assembled plasmids in *E. coli* showed the desired band after colony PCR (Fig.12) and were further confirmed though sequencing. However, the electroporation in *K. sucrofermentans* was unsuccessful. Only one plasmid, pSEVA331-P_{Lux}-*motB*, could be electroporated. However, the lack of cellulose production and the absence of PCR amplification of the *bcsA* gene, all indicate that probably the transformed strain was not *K. sucrofermentans* but probably a contaminant.

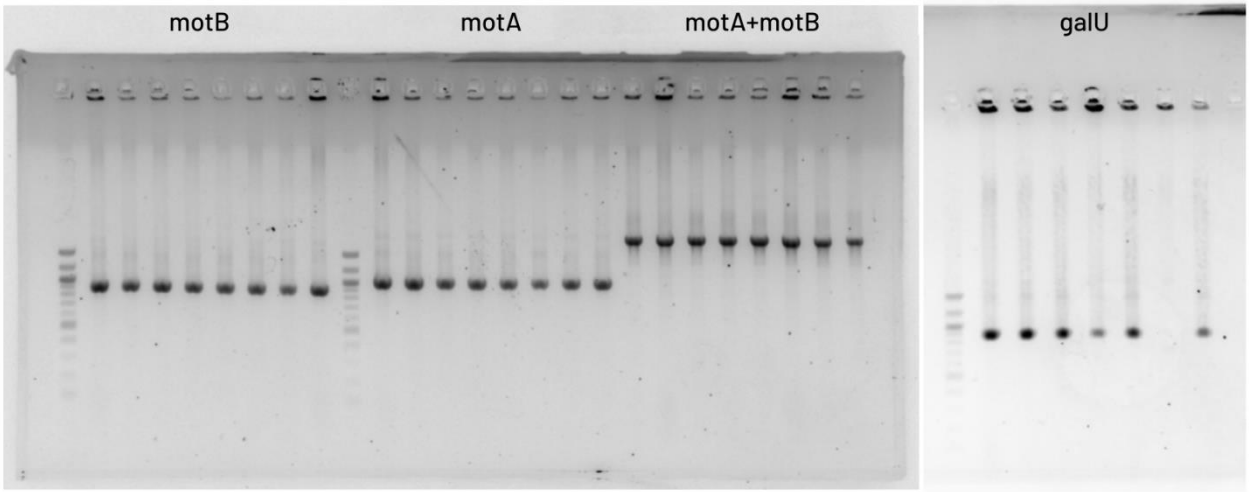

Figure 13. colony PCRs of the Gibson-assembled target plasmids. **By using the Gibson_gal/mot_fw and the Gibson_P_{Lux} _rv primers, all the desired bands (GeneRuler 100 bp Plus DNA ladder) were obtained for the following plasmids: pSEVA331-P_{Lux}-*motB* (1228 bp), pSEVA331-P_{Lux}-*motA* (1313 bp), pSEVA331-P_{Lux}-*motA-motB* (2301 bp) and pSEVA331-P_{Lux} -*galU* (1117 bp).**

4.3 P_{Lux} plate reader assay.

The plate reader results are summarized in Figure 14. The uninduced sample (0 µM) was not included in this graph, as it showed no growth (caused by a technical error). The 10 µM sample shows, from the start, a lower value than expected, probably due to a technical error. All the other samples, except for the 5 µM and 200 µM, showed positive correlation between inducer concentration and GFP/OD_{600} value. The standard deviation was particularly high in all of the samples treated with high concentration of HSL (200-800 µM), indicating high variability in the measurements.

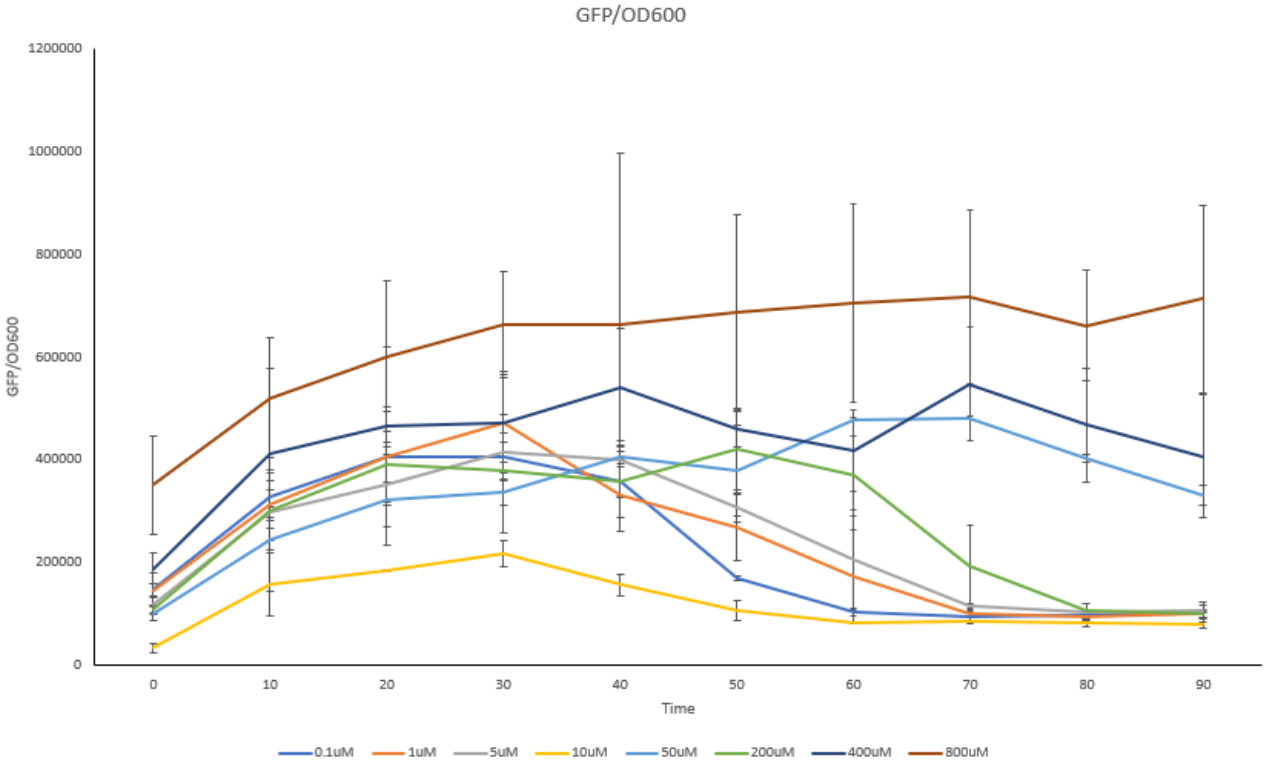

***Figure 14. GFP/OD_{600} measurement*. The time is expressed in hours. These measurements were obtained by dividing the measured GFP value for the OD_{600} value at the same time point. The obtained values were subtracted from the M9 value (M9 medium without any cells). The most representative time points were taken to simplify the graph, the original graph with all the time points can be found in Supplementary (Figure S4).**

OD_{600} plots (Fig.15) reveal that high concentrations of the inducer caused an inhibition in growth: this is clear for the 50 µM, 400 µM and 800 µM samples, but not for the 200 µM sample, indicating that the results obtained for this sample could be a result of a technical error in the preparation of the 200 µM concentrated stock. This same error can have also been made for the 10 µM sample, as it shows growth, but low induction compared to the other less concentrated samples.

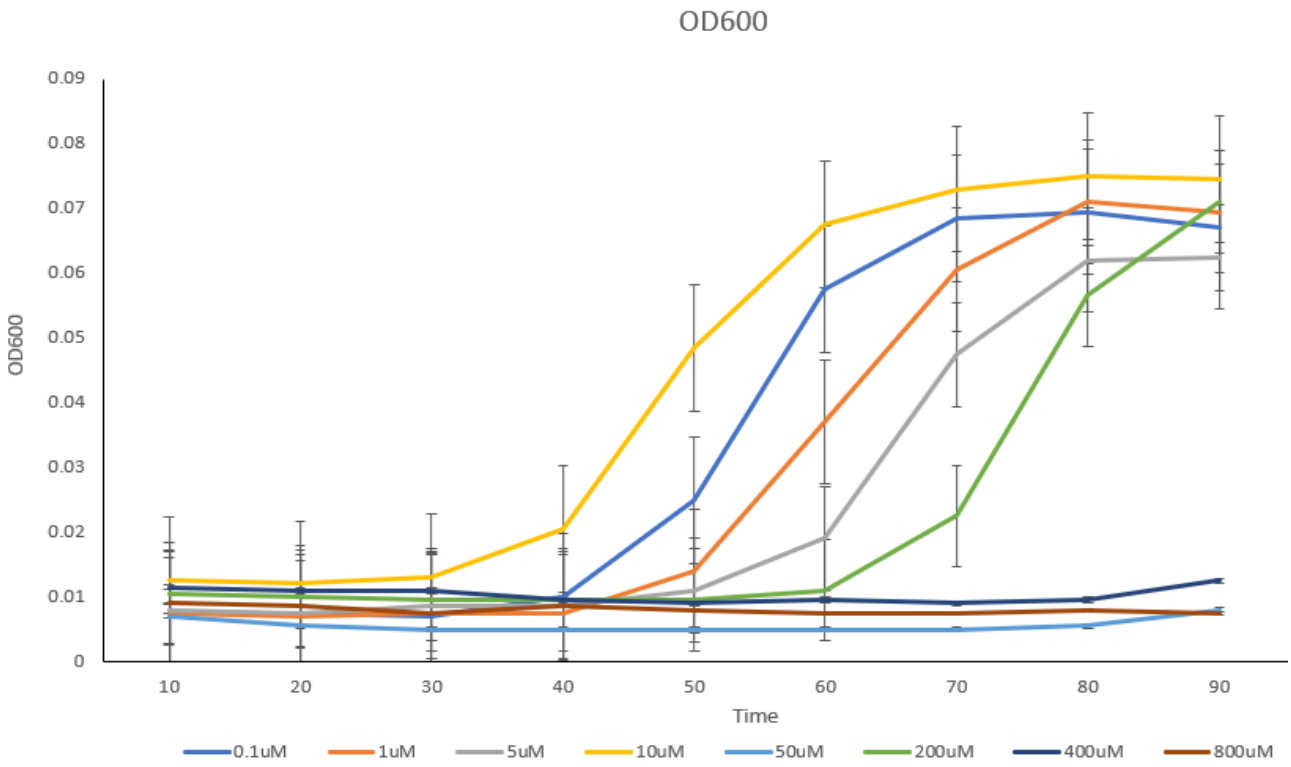

***Figure 15. OD600 graph of the uninduced and induced samples*. The time is expressed in hours. All values were subtracted from the M9 measurement. The most representative values were taken for each time point. The original graph can be found in the Supplementary (Figure S5).**

Since it showed no growth, the plate reader experiment for the 0 µM sample was repeated, this time with a positive outcome (Figure 16). The low standard deviation values indicate a low variability among the technical duplicates.

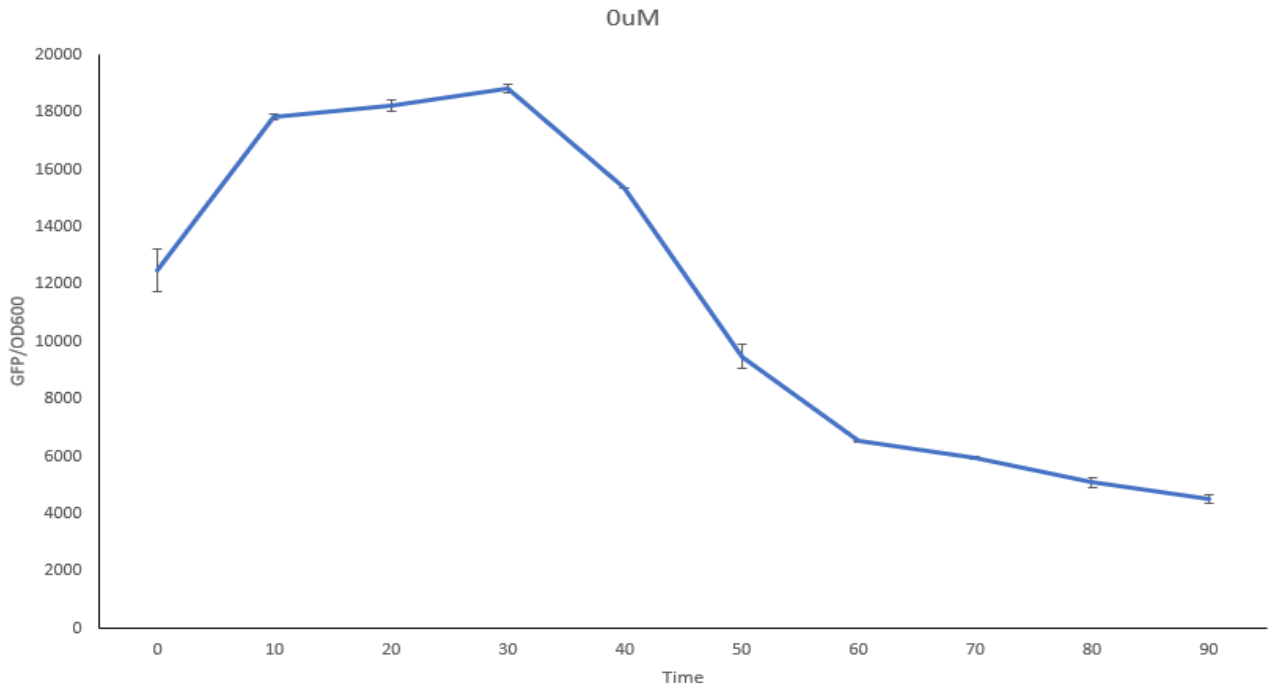

Figure 16. GFP/OD600 measurement of the uninduced sample. **The time is expressed in hours. These measurements were obtained by dividing the measured GFP value for the OD600 value at the same time point. The OD600 values were subtracted from the M9 value (M9 medium without any cells). The most representative values were taken for this graph. The original graph can be found in the Supplementary (Figure S8)**

5. Discussion

5.1 BC production on different carbon sources

From the BC growth, the fructose grown sample showed the thickest cellulose, the lowest change in pH in the medium and the highest OD600 after three days. This suggests that higher yields could be generated through growth on fructose, as the other samples' pH dropped to a point at which BC growth stops.

The results from the SEM analysis and the mass density method for porosity measurement indicate that these two methods are not equally reliable. This outcome is in line with a previous study conducted using BC, in which the values obtained using SEM deviated from the values using mass-density method (Hossen et al., 2020). As a consequence, these two methods do not complement each other but rather represent two distinct types of measurement of porosity, of which SEM seems ideal to assess pores' architecture and area in a specific point, while the mass-density method gives a more general view of the overall sample.

Through the mass-density method, the difference between the porosity of glucose, fructose and sucrose grown samples proved to be statistically significant ($p<0.05$) when grown at the same pH (6.5). However, these results contradict previous research conducted in *G.*

hansenii, in which fructose had the highest porosity among the three, while glucose the lowest (Ashrafi et al., 2019). Through the mass-density method, it was determined that the glucose samples had the highest average porosity, followed by fructose and sucrose. The difference between these results and literature could be explained by the fact that a different bacterial cellulose-producing strain was used. Another possible explanation is a different method for assessing porosity was used, namely Bubble Point test and Capillary Flow Porometry.

Though SEM, the average pore area was very similar between fructose, sucrose and the second glucose grown samples, indicating that the different carbon sources might not affect this parameter, as these samples were all grown the same day and in the same conditions. Additionally, it was expected the fructose-grown sample to have the highest average pore area, having the highest percentage of measured porosity. However, the average pore area was of 0.041 μm^2, even lower than the 96% porosity of the second glucose-grown sample. The first glucose-grown sample had a higher average pore area but was grown on a lower starting pH (5.5) due to a technical error in the media preparation. Consequently, different pH might affect pore areas and should be further studied as parameter. Another fact to take into account is the limitation of this measurement, as different images taken from the same sample proved to be significantly different ($p<0.05$). This indicates that the measurement has many limitations, partly dependent on the choice of the particular spots in which the images were taken, and the fact that this measurement focuses only on a very small part of the sample.

Overall, both mass-density method and SEM analysis have many limitations in porosity determination. The mass-density method seems to a better indicator of the capacity to retain water, rather than overall porosity, as the high percentage of porosity is not reflected on a higher area covered by pores compared to BC fibrils, as it is clearly visible from the SEM images. SEM analysis, instead, focuses only on a particular point of the BC cross section, and the pore sizes of the overall sample cannot be determined.

In general, different porosity assessment methods are already present but there is not yet a standard method, making a perfect porosity determination hard to achieve. A possible better alternative could be Capillary Flow Porometry. This relatively novel technique uses an instrument called porometer to measure pore size and pore size distribution of through pores, where the wetting liquid is displaced from the pores of a porous material by applying pressurized gas (Bonnier, 2025). Unfortunately, this method could not be tested in these experiments.

5.2 Cloning

All the desired plasmids were successfully assembled in *E. coli*. However, the majority of them could not be electroporated in *K. sucrofermentans*, indicating that the current electroporation protocol is not working efficiently. A conjugation protocol was recently developed by the iGEM 2025 BCoated team but could not be tested for this experiment. As a result, the impact of the genes overexpression could not be assessed. Only the pSEVA331-P_{Lux}-*GFPuv* plasmid was successfully electroporated, allowing the plate reader assay to be performed.

5.3 Plate reader assay

From the plate reader results, it can be concluded that high concentrations of inducer result on high GFPuv expression but also inhibition of growth. This pattern didn't occur for the 200 µM concentrated sample, indicating that a technical error might have occurred in the preparation of this sample. This same error can have also been made for the 10 µM sample, as it shows growth, but low induction compared to the other less concentrated samples. The unexpected results could have also been determined by the fact that the assay was performed using a 96-well plate with clear bottom and wells. This might have caused fluorescence to scatter and, therefore, determine higher fluorescence in some samples, derived from the scattering of the higher fluorescence samples. This statement is further emphasized by the fact that the standard deviation for the high concentrated samples is particularly high: the high variability can be explained by the fact that the fluorescence scattering has caused problems in the fluorescence measurement.

Last, the overall assay should be performed again using a 96-well plate with black bottom. It will also be important to make sure that the 0 µM sample grows on the same day, to have comparable results and subtract this value to the other values to have a better indication of the inducer effect.

6. Future Perspectives

The overall results give an indication of future studies that might be worth carrying out. From a production point of view, the difference between yield of glucose and fructose grown samples should be evaluated, as samples grown on fructose showed, in these preliminary results, to have higher thickness and lowest change in pH. As a result, it might be that fructose is preferable as a carbon source to grow cellulose in *K. sucrofermentans*, and confirming it would be valuable to improve BC production.

The difference in measured pore size of the first glucose grown sample indicates that different pH could affect porosity. Consequently, it would be interesting to study how different pH could affect porosity.

Future studies should focus on embedding compounds of different sizes. This could be done, for example, by taking comparable samples, incubating them with different compounds and recording the weight before and after the incubation. The results obtained should be compared to the results of the SEM analysis, and an evaluation between the pore area and compound embedment would be valuable. After embedment, it would be interesting to compare the release rates of these compounds and their possible correlation with pore size. This could be done by developing a biosensor, for accurate measurement.

Different methods to assess porosity should also be investigated, such as Capillary flow Porometry or Bubble Point test.

Additionally, the electroporation protocol was inefficient, and future studies should focus on optimizing the transformation of *K. sucrofermentans*. The conjugation protocol developed by the iGEM 2025 BCoated team could be tested, as it might have a higher efficiency. Once the transformation protocol is perfectioned, all the constructs should be tested in *K. sucrofermentans*, by growing BC at the same condition but with different concentrations of HSL inducer. The obtained BC should be tested for changes in porosity and pore size, to assess if different expression levels of *galU*, *motA* and *motB* have an impact on porosity. From the results of previous literature, the porosity is expected to decrease with *galU* overexpression, and increase with *motA*, *motB* and *motA-motB* overexpression. Additionally, since *galU* is directly involved in the BC production pathway, the possible changes in cellulose yield and productivity should be evaluated, according to the protocol provided by the iGEM 2025 BCoated team. The yield can be assessed by dividing BC dry weight for the weight of consumed glucose. The overall productivity can be evaluated by measuring the BC titer, by dividing the BC dry weight for the volume of fermentation broth, and divide the obtained value for the amount of incubation days.

The plate reader assay should also be performed again, using a 96-well plate with back bottom. Since very high concentrations of inducer showed strong inhibition of growth, the new experiment should use 200 µM as maximum value, and test multiple lower inducer concentrations.

7. Conclusion

Overall, through the mass-density method, glucose-grown samples showed the highest porosity, followed by fructose and sucrose. Notably, these results are in contrast with previous literature, probably because the strain used was different. In contrast, when looking at the SEM image analysis, there was not enough evidence that samples grown on glucose,

fructose and sucrose have a significant difference in pore area. However, the SEM analysis proved to be inaccurate, as different pictures taken from the same sample had significantly different average pore areas. These results indicate that these methods are not comparable and other porosity measurements, such as Capillary Flow Porometry, should be considered. This last method should be tested, and compared to the mass-density method, to assess changes in porosity based on carbon source and on the overexpression of *galU*, *motA*, and *motB* under the inducible promoter P_{Lux}. These genes overexpression could not be tested, due to the inefficiency of the electroporation protocol for *K. sucrofermentans*, but the results from the plate reader assay of *K. sucrofermentans* transformed with the plasmid pSEVA331-P_{Lux}-*GFPuv* suggest that concentrations higher than 50 µM of HSL cause a very strong induction but also a strong inhibition in growth. This will be important to consider when inducing the target genes with HSL.

8. Supplementary

Name	Type	Use	Features
pSEVA331	Plasmid backbone	Backbone for the pSEVA331-P_{Lux}-*GFPuv* assembly and all the derived assemblies	2968 bp; oriT, chloramphenicol resistance

pSEVA64-*gfpuv-LuxRwt*	Plasmid	Assembly of pSEVA-P_{Lux} - *GFPuv*, to insert *GFPuv* and partial fragment of *LuxR*	4985 bp; pRO1600 oriV, Gentamycin resistance
***LuxR* fragment**	DNA fragment (ordered from GenScript)	Assembly of pSEVA-P_{Lux}-*GFPuv*, to form a complete *LuxR* fragment and P_{Lux}	927 bp; P_{Lux} sequence, *LuxR* fragment under the J23100 constitutive promoter
pSEVA331- P_{Lux}-*GFPuv*	Assembled plasmid	Assembly of *motA*, *motB*, *motA-motB* and *galU* under the P_{Lux} inducible system	4723 bp; oriT, chloramphenicol resistance

***Table S1. Templates used for Gibson assemblies*. These templates were used for the assembly of pSEVA331- P_{Lux}-*GFPuv* and, from that, of pSEVA331-P_{Lux}-*galU*, pSEVA331-P_{Lux}-*motA*, pSEVA331-P_{Lux}-*motB* and pSEVA331-P_{Lux}-*motA-motB*.**

Primer	Template	Use	Sequence (5'-)	Tm (°C)
pSEVA331_T0_fw	pSEVA331	Gibson assembly	cttggactcctgttgatagatc	62
pSEVA331_T1_rv	pSEVA331	Gibson assembly	ggcatcaaataaaacgaaagg	59
Lamdba_T0_fw	pSEVA64-*gfpuv-LuxRwt*	Gibson assembly	cctttcgttttatttgatgccATTGGGGACCCCTGGATTC	67

rrnb_T1_rv	pSEVA64-*gfpuv-LuxRwt*	Gibson assembly	gatctatcaacaggagtccaagCTAGGGCGGCGGATTTG	67
Gibson_fw	pSEVA331- P_{Lux} -*GFPuv*	Colony PCR	ATTCCAGAAATCATCCTTAGC	50
Gibson_rv	pSEVA331- P_{Lux} -*GFPuv*	Colony PCR	cctggattctcaccaataaa	50
GFP_LuxR_fw	pSEVA64-*gfpuv-LuxRwt*	Gibson assembly	AACAAGAATTGGGACAACT	58
GFP_RBS_fw	*LuxR* fragment	Gibson assembly	AACAAGAATTGGGACAACTCCAGTGAAAAGTTCTTCTC	57
LuxR_rv	*LuxR* fragment	Gibson assembly	GGATGATTTCTGGAATTTATTAatttttaaagtatgggcaatc	55
galU_fw	*K.sucrofermentans* genome	Gibson assembly	CCGGactgTTATTTGTAGAGTGCCTGAAGCTCATTTATAC	61
galU_rv	*K.sucrofermentans* genome	Gibson assembly	agtaaagaggagaaaacagtGGTAAATATTAGTGATCAAGCC	58
motA_fw	*K.sucrofermentans* genome	Gibson assembly	agtaaagaggagaaaacagtATTAAGGAAACCATTGCGTG	61
motA_rv	*K.sucrofermentans* genome	Gibson assembly	CCGGactgTTATTTGTAGAAATAACCCTTGCCTTGGTC	64
motB_fw	*K.sucrofermentans* genome	Gibson assembly	agtaaagaggagaaaacagtAAGGCAAGGGTTATTTCATG	60
motB_rv	*K.sucrofermentans* genome	Gibson assembly	CCGGactgTTATTTGTAGACTTTTGATCCTGATTCTTGC	60
GFP_gal/mot_fw	pSEVA331-P_{Lux}-*GFPuv*	Gibson assembly	actgttttctcctctttact	57
GFP_gal/mot_rv	pSEVA331-P_{Lux}-*GFPuv*	Gibson assembly	CAAAAAAGGGCAAGGTCTAG	61
Gibson_gal/mot_fw	pSEVA331-P_{Lux}-*galU/motAB*	Colony PCR	gtCCAAGACTAGACCTTGCc	57
Gibson_P_{Lux}_rv	pSEVA331-P_{Lux} -*galU/motAB*	Colony PCR	gtatgtgtcgtcggcatttatg	55

***Table S2. Primers used and sequences*. The overhangs for Gibson assembly are highlighted in red. The Tm was determined with the NEB Tm calculator, using Q5 for the PCRs for Gibson assembly and OneTaq Hot Start for the colony PCRs.**

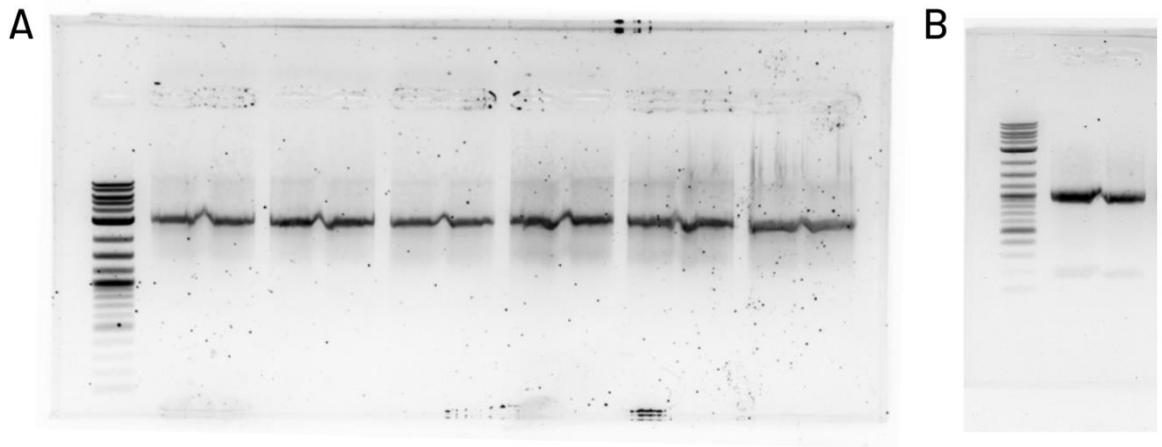

***Figure S1. PCR amplification of the pSEVA331 backbone and of the pSEVA64-gfpuv-LuxRwt fragment*. A. The ladder (GeneRuler 1kb DNA ladder) indicates the presence of the desired pSEVA331 band (2.8kb), which was subsequently isolated from the gel. Primers used: pSEVA331_T0_fw +**

pSEVA331_T1_rv. B. The ladder indicates the presence of the desired pSEVA64 band (1.9kb), which was subsequently isolated from the gel. Primers used: Lambda_t0_fw + rrnb_T1_rv.

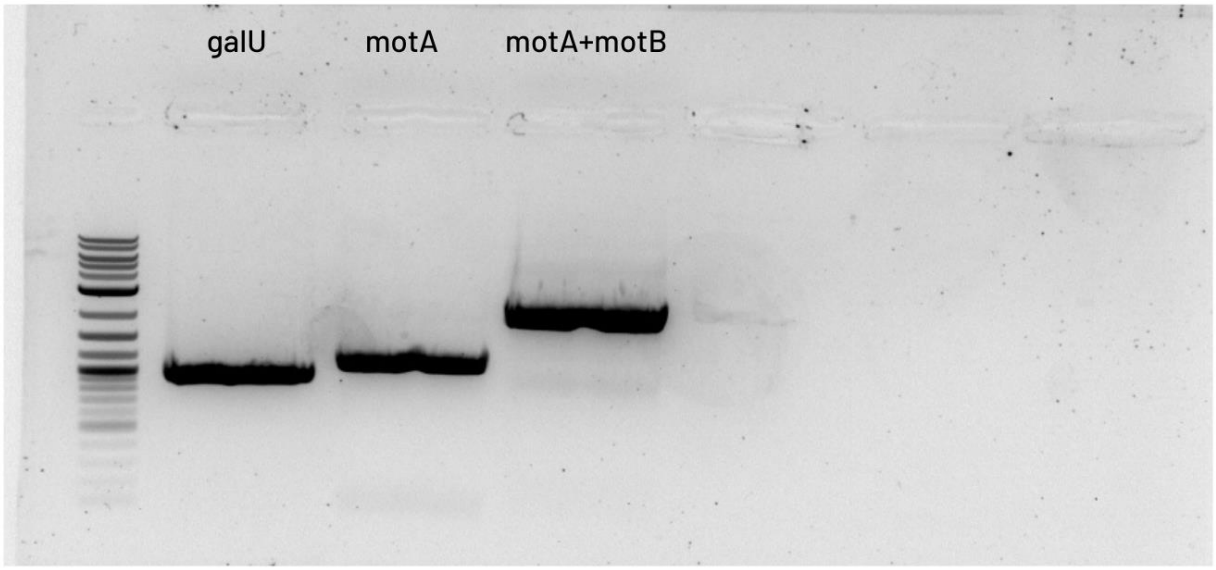

***Figure S2. PCR (Q5) of target genes from K. sucrofermentans*. All the amplified fragments showed the desired bands: *galU* (931bp), *motA* (1127bp) and *motA+motB* (2115bp).**

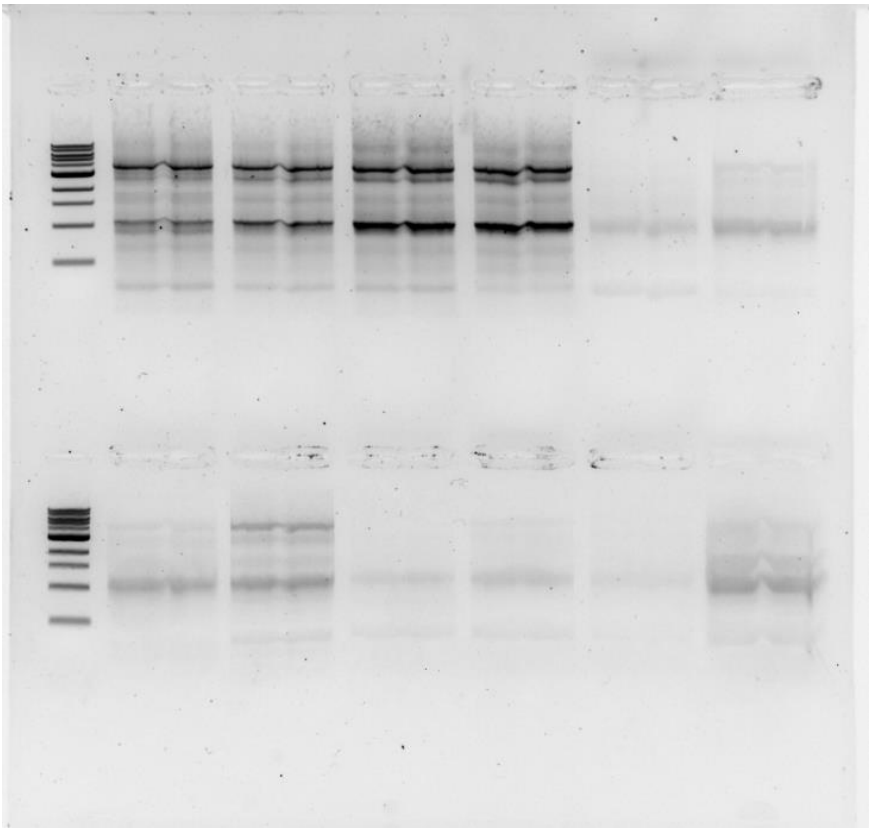

***Figure S3. amplification of pSEVA331-*P_{Lux}*-GFPuv for Gibson assembly*. The desired band (3998 bp) is shown together with multiple other bands (probably caused by the presence of other binding sites for one of the plasmids).**

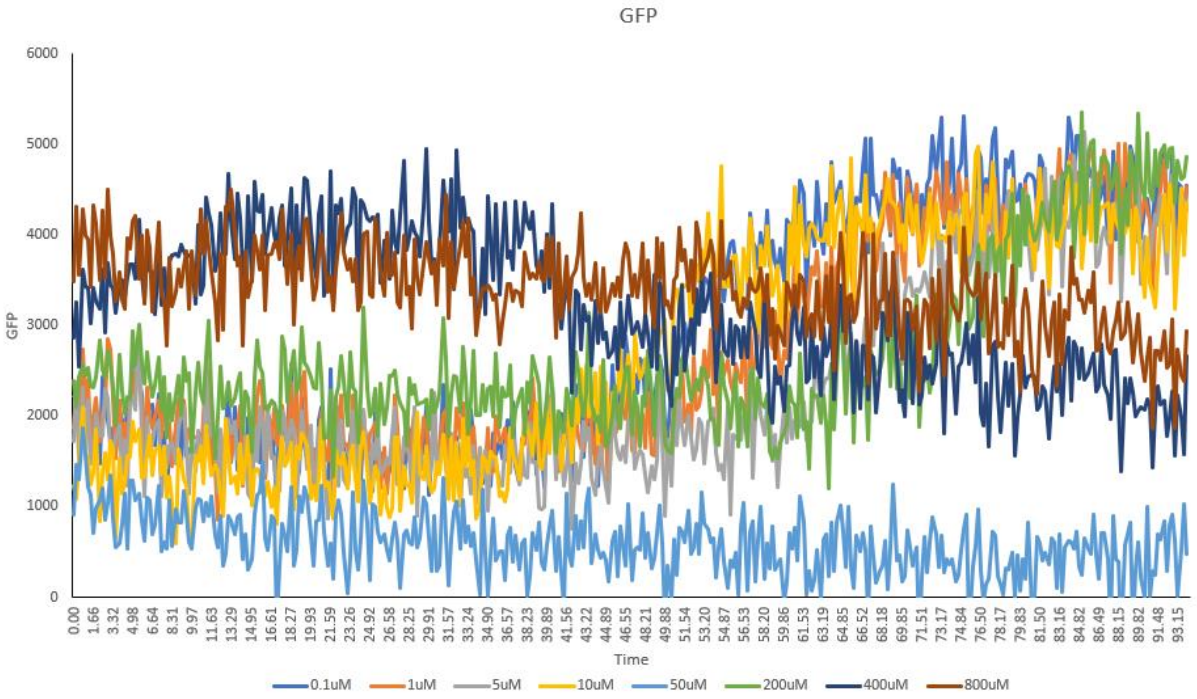

***Figure S4. Fluorescence plate reader data*. This data was obtained using all the GFP measurements recorded subtracted from the M9 value (only medium).**

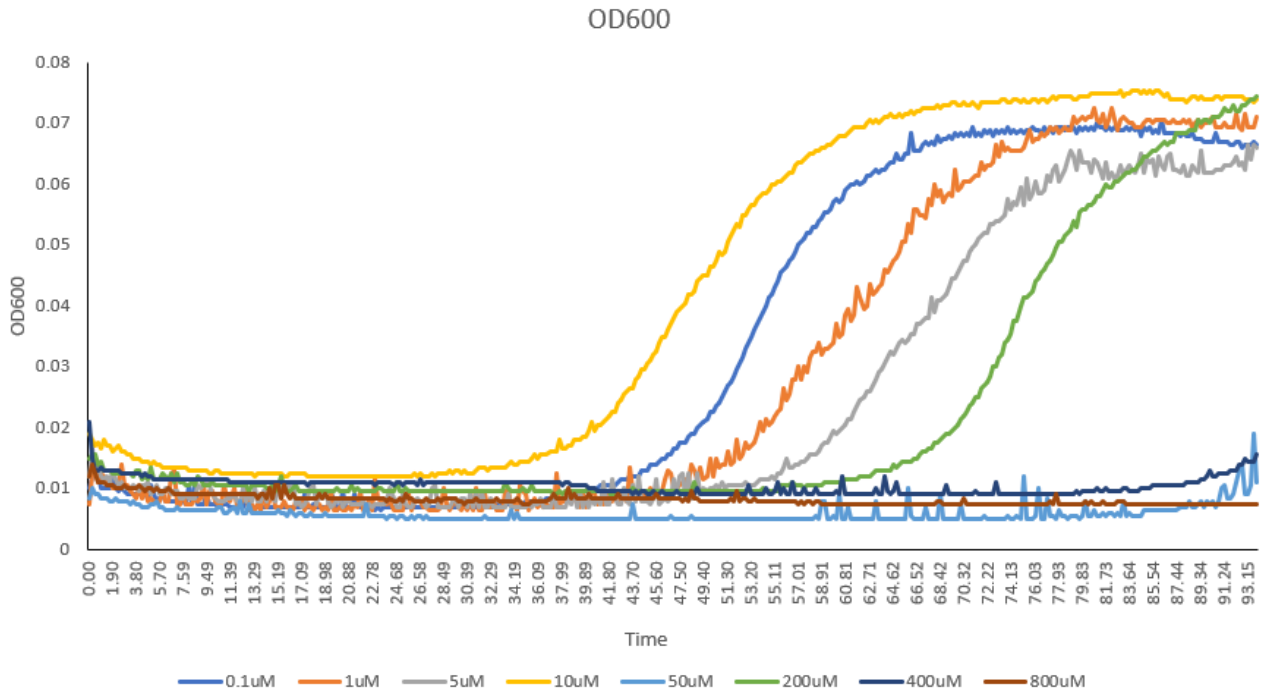

***Figure S5. OD$_{600}$ measurement*. All values were subtracted from the M9 value (only medium). The time is expressed in hours.**

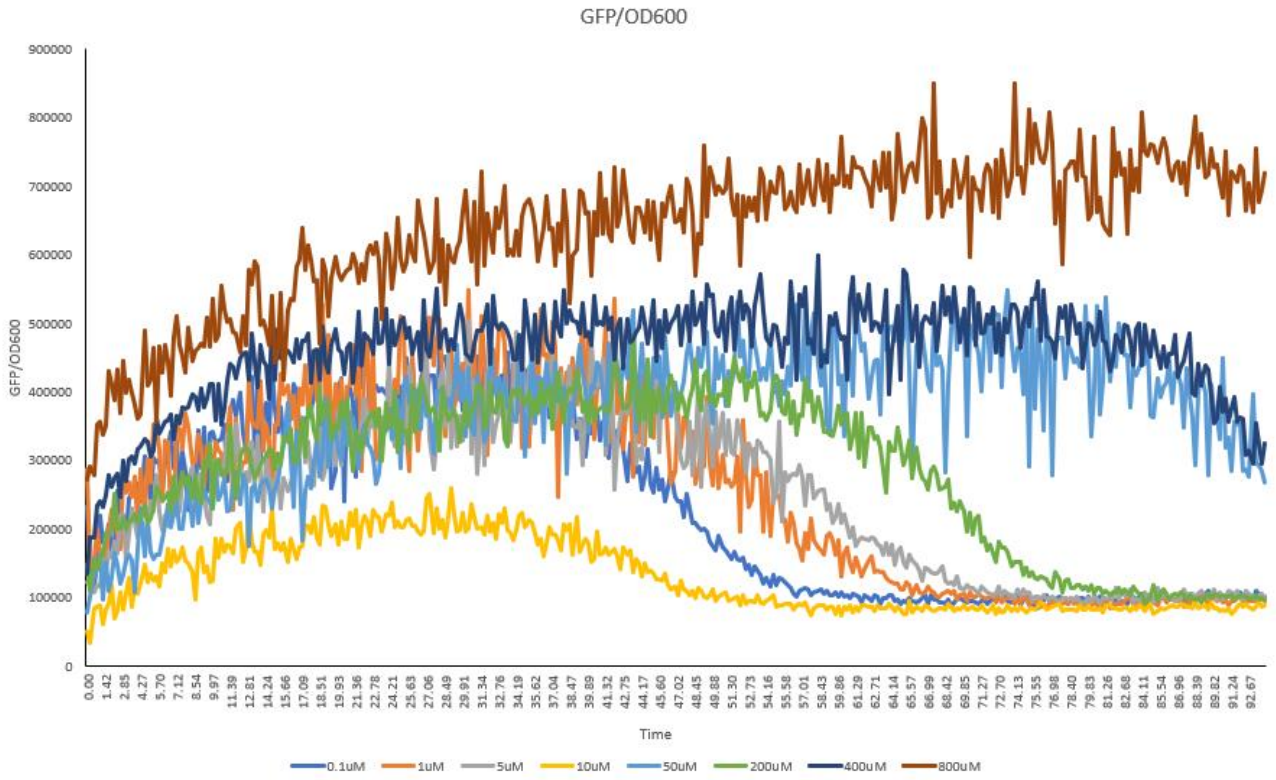

Figure S6. Complete GFP/OD600 plate reader measurements. **This graph contains all data points and was obtained subtracting the M9 value (only medium). The time is expressed in hours.**

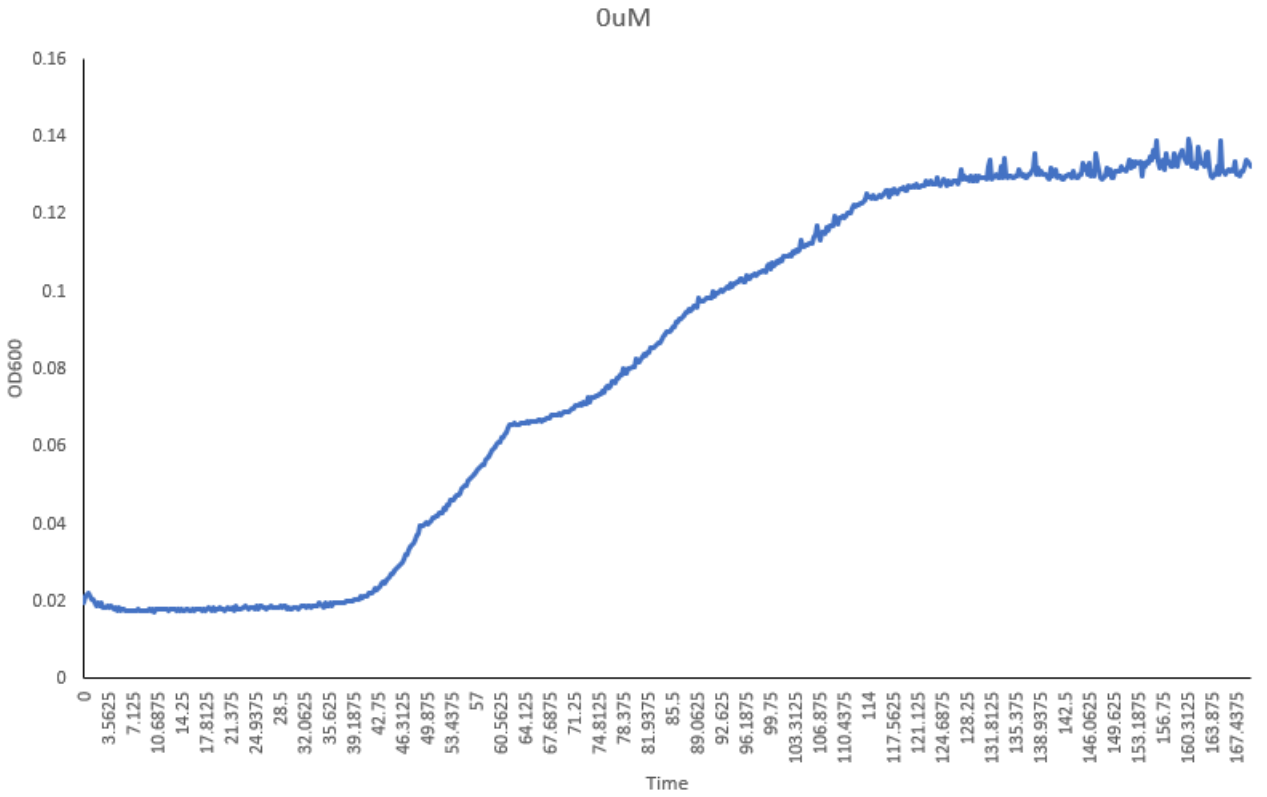

Figure S7. OD600 measurement for the 0 µM sample. **This graph contains all data points and was obtained subtracting the M9 value (only medium). The time is expressed in hours.**

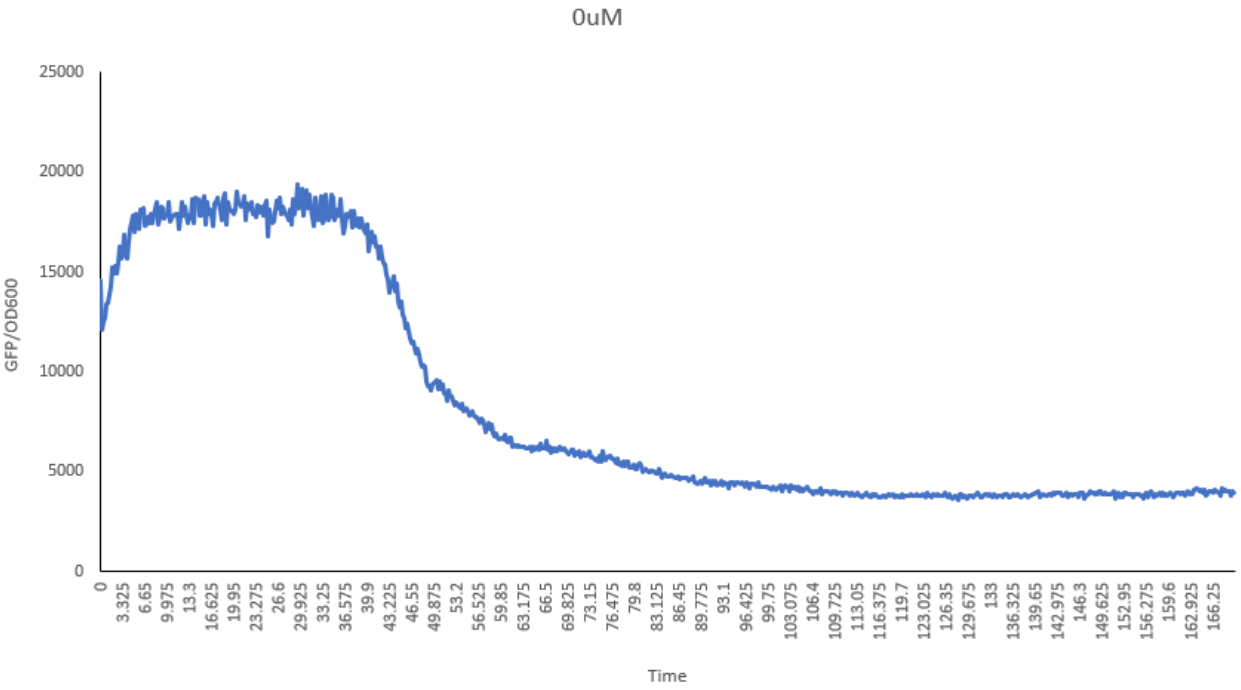

Figure S8. GFP/OD$_{600}$ measurement for the 0 µM sample. **This graph contains all data points, with the OD$_{600}$ value obtained subtracting the M9 value (only medium). The time is expressed in hours.**

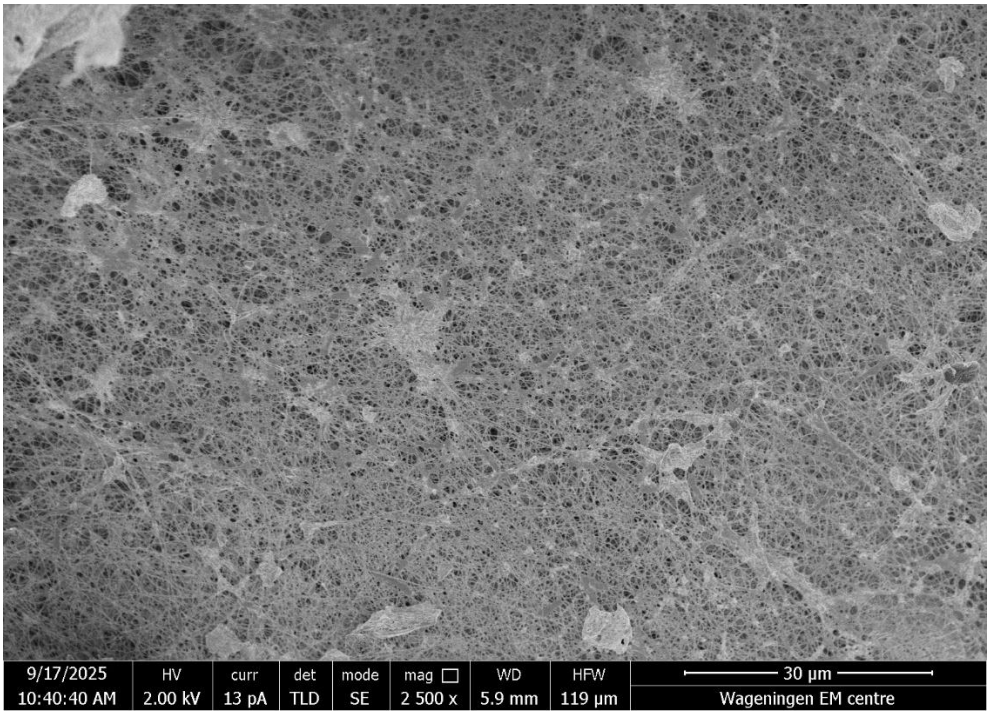

Figure S9. Image of the cross section in which the SEM images were taken for the second glucose-grown sample.

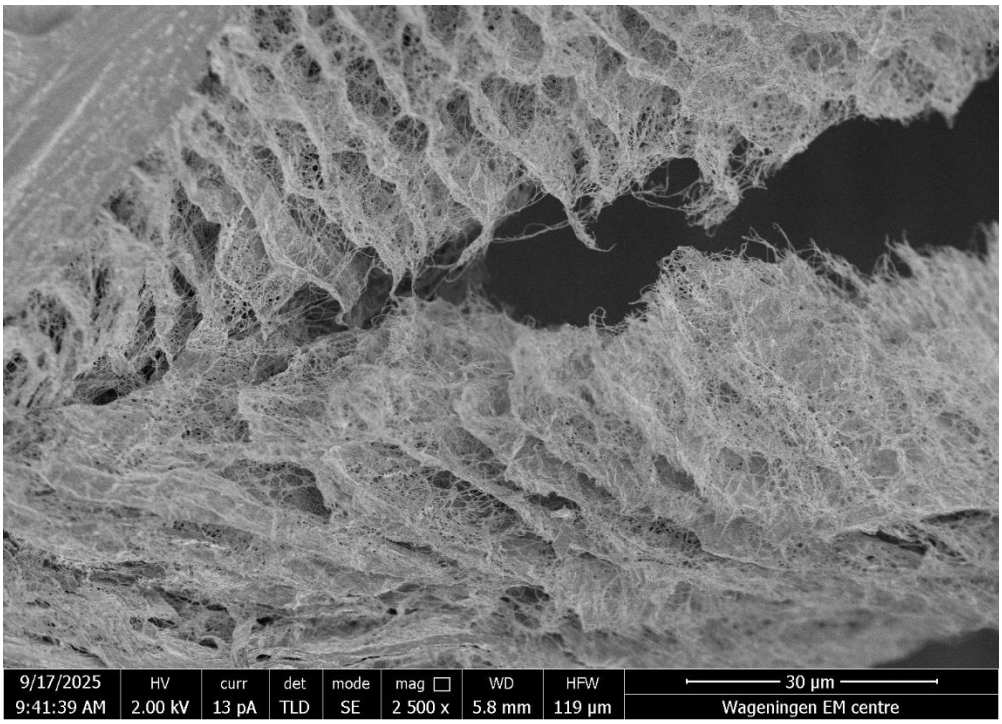

Figure S10. Image of the cross section in which the SEM images were taken for the first glucose-grown sample.

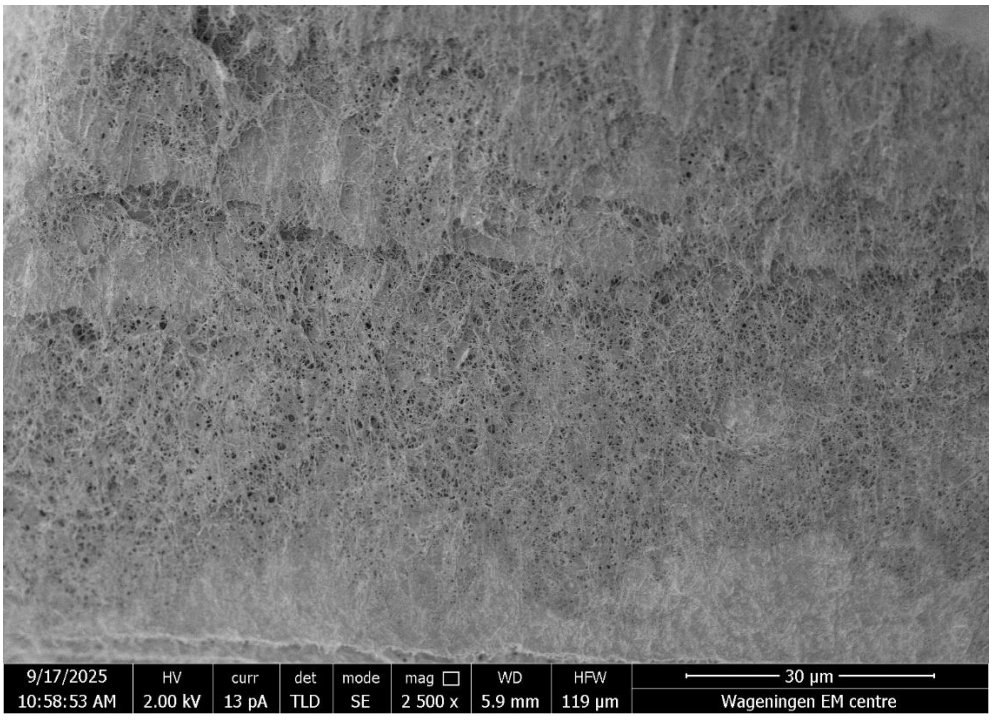

Figure S11. Image of the cross section in which the SEM images were taken for the fructose-grown sample.

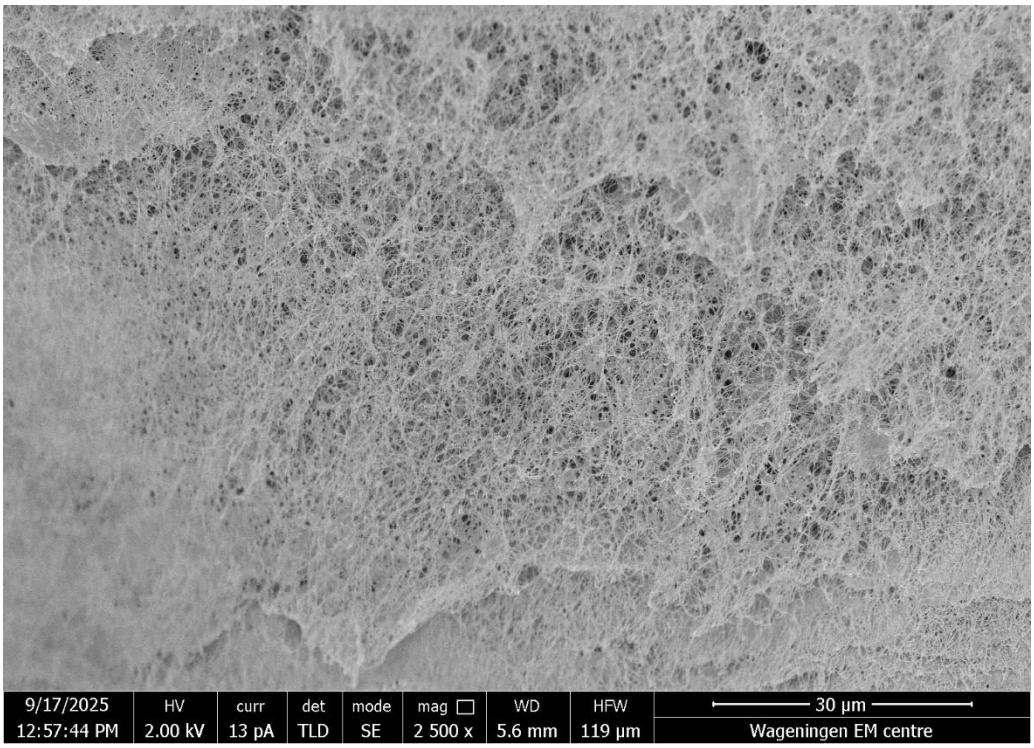

Figure S12. Image of the cross section in which the SEM images were taken for the sucrose-grown sample.

References

Andreola, F., Leonelli, C., Romagnoli, M., & Miselli, P. (2000). Techniques used to determine porosity. *American Ceramic Society Bulletin, 79*, 49–52.

Ashrafi, Z., Lucia, L., & Krause, W. (2019). Bioengineering tunable porosity in bacterial nanocellulose matrices. *Soft matter*, *15*(45), 9359–9367. https://doi.org/10.1039/c9sm01895f

de Amorim, J. D. P., da Silva Junior, C. J. G., de Medeiros, A. D. M., do Nascimento, H. A., Sarubbo, M., de Medeiros, T. P. M., Costa, A. F. S., & Sarubbo, L. A. (2022). Bacterial Cellulose as a Versatile Biomaterial for Wound Dressing Application. *Molecules (Basel, Switzerland)*, *27*(17), 5580. https://doi.org/10.3390/molecules27175580

Basu, A., Vadanan, S. V., & Lim, S. (2018). A Novel Platform for Evaluating the Environmental Impacts on Bacterial Cellulose Production. *Scientific reports*, *8*(1), 5780. https://doi.org/10.1038/s41598-018-23701-y

Betlej, Izabela & Zakaria, Sarani & Krajewski, Krzysztof & Boruszewski, P.. (2021). Bacterial Cellulose - Properties and Its Potential Application. Sains Malaysiana. 50. 493-505. 10.17576/jsm-2021-5002-20

Bogino, P. C., Oliva, M.deL., Sorroche, F. G., & Giordano, W. (2013). The role of bacterial biofilms and surface components in plant-bacterial associations. *International journal of molecular sciences*, *14*(8), 15838–15859. https://doi.org/10.3390/ijms140815838

Bonnier, J. (2025, July 9). *How capillary flow porometry works*. Porometer. https://www.porometer.com/knowledge-center/news/capillary-flow-porometry-porometer

Brown RM, Willison JH, Richardson CL. Cellulose biosynthesis in Acetobacter xylinum: visualization of the site of synthesis and direct measurement of the in vivo process. Proc Natl Acad Sci U S A. 1976;73:4565–4569. doi: 10.1073/pnas.73.12.4565

El-Gendi, H., Taha, T., Ray, J., & Saleh, A. (2022). Recent advances in bacterial cellulose: A low-cost effective production media, optimization strategies, and applications. Cellulose. https://doi.org/10.1007/s10570-022-04697-1

Gregory, D. A.; Tripathi, L.; Fricker, A. T. R.; Asare, E.; Orlando, I.; Raghavendran, V.; Roy, I. Bacterial Cellulose: A Smart Biomaterial with Diverse Applications. *Carbohydrate Polymers* **2021**, *252*, 117202. **https://doi.org/10.1016/j.carbpol.2020.117202**

Hossen, M. I., Rautkari, L., Honkanen, M., Sirviö, J. A., & Korpela, A. (2020). A comparative study of methods for porosity determination of cellulose based porous materials. Cellulose, 27(12), 7007–7021. https://doi.org/10.1007/s10570-020-03262-8

Huang, L. H., Liu, Q. J., Sun, X. W., Li, X. J., Liu, M., Jia, S. R., Xie, Y. Y., & Zhong, C. (2020). Tailoring bacterial cellulose structure through CRISPR interference-mediated downregulation of galU in Komagataeibacter xylinus CGMCC 2955. *Biotechnology and bioengineering*, *117*(7), 2165–2176. https://doi.org/10.1002/bit.27351

ImageJ. (2020, January 24). *What is binarization and what is it good for?* In *Principles*. ImageJ. https://imagej.net/imagej-wiki-static/Principles.html#What_is_binarization_and_what_is_it_good_for.3F

Jacek, P., Ryngajłło, M., & Bielecki, S. (2019). Structural changes of bacterial nanocellulose pellicles induced by genetic modification of Komagataeibacter hansenii ATCC 23769. *Applied microbiology and biotechnology*, *103*(13), 5339–5353. https://doi.org/10.1007/s00253-019-09846-4

Römling, U., & Galperin, M. Y. (2015). Bacterial cellulose biosynthesis: diversity of operons, subunits, products, and functions. Trends in microbiology, 23(9), 545–557. https://doi.org/10.1016/j.tim.2015.05.005

de Souza, S.S., Berti, F.V., de Oliveira, K.P.V. *et al.* Nanocellulose biosynthesis by *Komagataeibacter hansenii* in a defined minimal culture medium. *Cellulose* **26**, 1641–1655 (2019). https://doi.org/10.1007/s10570-018-2178-4

Swingler, S., Gupta, A., Gibson, H., Kowalczuk, M., Heaselgrave, W., & Radecka, I. (2021). Recent Advances and Applications of Bacterial Cellulose in Biomedicine. *Polymers*, *13*(3), 412. https://doi.org/10.3390/polym13030412

Tamar, E., Koler, M., & Vaknin, A. (2016). The role of motility and chemotaxis in the bacterial colonization of protected surfaces. *Scientific reports*, *6*, 19616. https://doi.org/10.1038/srep19616

Teh, M. Y., Ooi, K. H., Danny Teo, S. X., Bin Mansoor, M. E., Shaun Lim, W. Z., & Tan, M. H. (2019). An Expanded Synthetic Biology Toolkit for Gene Expression Control in Acetobacteraceae. *ACS synthetic biology*, *8*(4), 708–723. https://doi.org/10.1021/acssynbio.8b00168

Volova, T. G., Prudnikova, S. V., Kiselev, E. G., Nemtsev, I. V., Vasiliev, A. D., Kuzmin, A. P., & Shishatskaya, E. I. (2022). Bacterial Cellulose (BC) and BC Composites: Production and Properties. *Nanomaterials (Basel, Switzerland)*, *12*(2), 192. https://doi.org/10.3390/nano12020192

Zhong, C. Industrial-Scale Production and Applications of Bacterial Cellulose. *Frontiers in Bioengineering and Biotechnology* 2020, *8*. https://doi.org/10.3389/fbioe.2020.605374